NTNU
Norwegian University of
Science and Technology

Alloys as Anode Materials in Magnesium Ion Batteries

Alf Petter Syvertsen

Nanotechnology
Submission date: Januar 2012
Supervisor: Fride Vullum, IMTE

Norwegian University of Science and Technology
Department of Materials Science and Engineering

Abstract

This thesis is a feasibility study of the possible application of magnesium alloys for future magnesium-ion batteries. It investigates different alloys and characterizes them with respect to internal resistance, overpotentials and the reversibility of the electrochemical reaction. SEM and EDS studies of used electrodes have also been carried out. It has been showed that alloys, easier to handle and at a fraction of the cost, can be used with equal or better performance than pure Mg. The seemingly superior alloy, AZ61 exhibits a coloumbic efficiency close to 100%, at higher charge rates than pure Mg.

Acknowledgements

The electrode materials and electrolyte were provided by SINTEF and is acknowledged. The other materials for this project were provided by the Department of Materials Science and Engineering (IMT) at NTNU and is acknowledged. All equipment for the synthesis and characterization is property of the Department of Materials Science and Engineering (IMT) at NTNU and SINTEF and its use is acknowledged. Invaluable help and teaching assistance is acknowledged from Silje Rodahl at SINTEF. Also acknowledged for their contribution is my supervisor, Associate Professor Fride Vullum-Bruer, SINTEF-engineers Edel Sheridan and Anita Fossdal and Ph.D. candidate Morten Onsrud.

Contents

Table of Contents . . . 6

List of Figures . . . 8

List of Tables . . . 10

1 Introduction **11**

2 Theory **13**

2.1 Electrochemistry . . . 13

2.1.1 Electromotive Force . . . 13

2.1.2 Electrode Potential . . . 14

2.1.3 Energy Storage . . . 15

2.1.4 Charge Transfer and Overpotential . . . 15

2.2 Cyclic Voltammetry . . . 16

2.2.1 Extracting Data . . . 17

2.3 Battery Theory . . . 19

2.4 Lithium Batteries . . . 19

2.4.1 Anode Materials . . . 20

2.4.2 Electrolytes . . . 21

2.4.3 SEI-layer . . . 23

2.4.4 Cathode Materials . . . 23

2.5 Magnesium Batteries . . . 25

2.5.1 Theory . . . 25

2.5.2 Electrode Materials . . . 26

2.5.3 Electrolytes . . . 28

2.6 SEM and EDS . . . 29

3 Experimental **31**

3.1 Chemicals . . . 31

3.2 Equipment . . . 32

3.3 Electrolyte Preparation 32
  3.3.1 $(BuAlCl_3)_2Mg$ 32
  3.3.2 All Phenyl Complex 32
3.4 Electrode Preparation 33
  3.4.1 Metal Electrodes 33
  3.4.2 V_2O_5 34
3.5 Cell Assembly 34
  3.5.1 3-Electrode Cell 34
  3.5.2 Coin Cells 36
3.6 Measurements 36
  3.6.1 Initial Measurements 36
  3.6.2 Measurement Scheme 36
3.7 SEM 38

4 Results **39**
4.1 Measurements 39
  4.1.1 Cycles 39
  4.1.2 E^{rev} and Overpotentials 40
4.2 Initial Measurements 41
  4.2.1 Scan Speeds 41
  4.2.2 External Reference 41
  4.2.3 Internal Pressure 43
  4.2.4 Etching 44
4.3 Cyclic Voltammetry 46
  4.3.1 Pure Magnesium 47
  4.3.2 AZ31 48
  4.3.3 AZ61 49
  4.3.4 AT61 50
  4.3.5 AP65 51
  4.3.6 Untreated Alloys 52
  4.3.7 Intercalation Electrodes 53

4.4 Electrolyte Stability 54
4.5 SEM and EDS 54
  4.5.1 Mg 54
  4.5.2 AZ31 55
  4.5.3 AP65 56
4.6 Practical 56

5 Discussion **57**
5.1 External Reference 57
5.2 Kinetics 57
5.3 Internal Pressure 58
5.4 Etching 58
5.5 Charge Capacity and Efficiency 58
5.6 Resistance and Overpotentials 59
5.7 Deposit Structure and Composition 60
5.8 Effect of Alloying Elements 60
5.9 Intercalation Electrodes 61
5.10 Electrolyte Stability 61
5.11 Practical 61

6 Conclusion **63**

7 Further Work **65**
7.1 Extending This Thesis 65
7.2 Magnesium-ion Batteries 65

References **69**

A Materials and chemicals **71**

B EDS spectra **75**
B.1 Mg 75
B.2 AZ31e 77

B.3 AP65 79

List of Figures

2.1 A general outline of a galvanic cell. 15

2.2 Schematics of a standard electrochemical cell used in CV-experiments. 17

2.3 Typical CV experiments on a $Fe(CN)_6^{3-}/Fe(CN)_6^{4-}$ redox couple in water. 17

2.4 Illustration of data extracted from a CV of pure Mg vs. Cu. 18

2.5 Schematic of a general lithium-ion battery cell 20

2.6 The structural changes upon lithiation of graphite. 22

2.7 Typical electrochemical behavior and basic structure of $Mg_xMo_3S_4$. . 27

3.1 Comparison of electrodes before and after polishing 33

3.2 Schematics of the three electrode cell used in our experiments. . . . 35

3.3 Graphic presentation of the potential applied as a function of time. . 37

4.1 The 10th and 11th cycle of the AT61 specimen with 0.6 mm spacer. 39

4.2 A closeup around E^{rev} of the Mg electrode shown in Figure 4.9. . . . 40

4.3 The 11th cycle of a Mg-electrode at 20mV/s and the next cycle at 10mV/s. 42

4.4 The last cycles at 20mV/s with Mg (blue) and AZ61 (red) electrodes with Mg as an external reference. 42

4.5 The first runs of the AT61 with 0.6 mm spacer (blue) and 0.8 mm spacer (red). 43

4.6 The last runs of the AT61 with 0.6 mm spacer (blue) and 0.8 mm spacer (red). 44

4.7 The first runs of the $AZ31e_{0.8}$ (blue) and $AZ31_{0.6}$ (red) electrodes. . 45

4.8 The last runs of the $AZ31e_{0.8}$ (blue) and $AZ31_{0.6}$ (red) electrodes. . 45

4.9 The full cyclic voltammogram of the 20 cycles before failure for $Mg_{0.8}$. 47

4.10 The full cyclic voltammogram of the 11 runs for $AZ31e_{0.6}$. 48

4.11 The full cyclic voltammogram of the last 14 cycles for $AZ61e_{0.6}$. . . 49

4.12 The full cyclic voltammogram for $AT61_{0.8}$ for the first 20 cycles. . . 50

4.13 The last 21 cycles of the cyclic voltammogram of $AP65_{0.8}$. 51

4.14 Cyclic voltammograms of the four untreated alloys. 52

4.15 The second cycle of the CV's of Mg (green), AZ61e (red) and AZ61 (blue) vs. V_2O_5, cycled at 1 mV/s. 53

4.16 The LSV-sweep on the untreated alloys. Sweep rate 20 mV/s. 54

4.17 The two electrodes of an Mg-cell after cycling. Recorded at 15 kV. . 55

4.18 The two electrodes of an AZ31e-cell after cycling. Recorded at 5 kV. 55

4.19 The two electrodes of an AP65-cell after cycling. Recorded at 5 kV. 56

B.1 EDS data from the Mg-electrode in the $Mg_{0.8}$-cell. 75

B.2 EDS data from the Cu-electrode in the $Mg_{0.8}$-cell. 76

B.3 EDS data from the AZ31e-electrode in the $AZ31e_{0.6}$-cell. 77

B.4 EDS data from the Cu-electrode in the $AZ31e_{0.6}$-cell. 78

B.5 EDS data from the AP65-electrode in the $AP65_{0.8}$-cell. 79

B.6 EDS data from the Cu-electrode in the $AP65_{0.8}$-cell. 80

List of Tables

1.1 Key properties of selected elements. 11

2.1 Key properties of commonly used solvents in lithium-ion batteries. . 23

2.2 Typical lithium-ion cathode materials. 24

2.3 Key properties of magnesium 25

2.4 Key properties of the solvents used in the study. 28

3.1 Chemicals used in this thesis. 31

3.2 Magnesium alloys used in this thesis. The amount of alloying elements are given in wt%. 31

3.3 Equipment used during this thesis. 32

3.4 Sizes of the different cell components. 34

4.1 Comparison of the 11th cycle at 20mV/s and the 12th cycle at 10mV/s for a Mg-electrode 41

4.2 The reversible potential and overpotentials of Mg and AZ61 with an external Mg-reference. 41

4.3 Comparision of the effect of internal pressure measured on batteries assembled with AT61-electrodes and 0.6 mm or 0.8 mm spacers. . . 43

4.4 The resistance and charge extracted from the CV for AZ31e and AZ31 44

4.5 The reversible potential, peak anodic potential and the overpotentials for AZ31 and AZ31e. 44

4.6 The resistance and charge extracted from the CV of $Mg_{0.8}$ cycled at 20 mV/s. 47

4.7 The reversible potential, peak anodic potential and the overpotentials for $Mg_{0.8}$. 47

4.8 The resistance and charge extracted from the CV of $AZ31e_{0.6}$ cycled at 20 mV/s. 48

4.9 The reversible potential, peak anodic potential and the overpotentials for $AZ31e_{0.6}$. 48

4.10 The resistance and charge extracted from the CV of $AZ61e_{0.6}$ cycled at 20 mV/s. 49

4.11 The reversible potential, peak anodic potential and the overpotentials for AZ61e$_{0.6}$. 49

4.12 The resistance and charge extracted from the CV of AT61$_{0.8}$ cycled at 20 mV/s. 50

4.13 The reversible potential, peak anodic potential and the overpotentials for AT61$_{0.8}$. 50

4.14 The resistance and charge extracted from the CV of AP65$_{0.8}$ cycled at 20 mV/s. 51

4.15 The reversible potential, peak anodic potential and the overpotentials for AP65$_{0.8}$. 51

4.16 The results of the CV of AP65u$_{0.8}$ cycled at 20 mV/s 52

A.1 Materials and chemical used during this project 72

A.2 Full specifications of the magnesium alloys used in this thesis. 73

1 Introduction

Since Sony first patented and commercialized secondary lithium-ion (Li-ion) batteries in 1991 they have been developed and optimalized and is now the de-facto standard for rechargeable batteries in electrical consumer applications.

The battery market is also rapidly growing. As battery electric vehicles (BEV) and plug-in hybrid electric vehicles (PHEV) continue to increase in usability, their market share is rapidly increasing, pulling the battery market up together with it. The battery market has been growing steadily for the past 20 years and is expected to continue to grow at least as fast in the coming years [1].

While lithium-ion batteries is one of the most popular battery technologies of today, it faces several difficulties and one of the greatest is is scarcity of resources. William Tahil points out in his report, *The trouble with Lithium* [2] that if all the BEV and PHEV of the future would be powered by lithium-ion batteries there would not be enough lithium in the world to sustain even one year of production.

This calls for the need of new types of batteries without the underlying limitations concerning the lithium-ion battery technology. When judging a technology just by the active ion's underlying properties, the most important factors are; the reduction potential, atomic weight, ion size, valence and abundance. These factors are summed up in Table 1.1.

Table 1.1: Key properties of selected elements. Reduction potential is in aqueous solutions vs. SHE, weight is the average isotope weight, ionic radius is the crystal radiusfor a six-coordinate ion and abundance is the average composition in the earth's crust.

Element	E^o [3]	Weight	Ionic Radius [4]	Valence	Abundance [5]
Li	-3.00 V	6.9 u	0.90 Å	1	10 µg/g
Na	-2.71	23.0 u	1.16 Å	1	3.4 wt%
Mg	-2.38 V	24.3 u	0.86 Å	2	2.1 wt%
Al	-1.66 V	27.0 u	0.675 Å	3	19.0 wt%
K	-2.92 V	39.1 u	1.52 Å	1	2.0 wt%
Ca	-2.84 V	40.1 u	1.14 Å	2	5.4 wt&
Ti	-1.8 V	47.9 u	1.00 Å	2	0.48 wt%

Magnesium is a very good choices it offers a good trade-off between the mentioned factors. Magnesium-based batteries have also been subject to some research the last 20 years and the worldwide magnesium industry is already producing over 700 000 tonnes a year, benefiting the research and production of this technology.

One of the big limitations with magnesium, however, is the very high price of pure magnesium. This is because it is usually found in minerals containing several other divalent atoms, and this makes it very hard to separate out the pure Mg. This thesis aims to explore the feasibility of using cheaper magnesium alloys as electrode materials in magnesium batteries.

2 Theory

2.1 Electrochemistry

The theory of electrochemistry is excellently presented in the book *Electrochemistry* by *C.H. Hamann, A. Hamnett* and *W. Vielstich* [6]. Here a summary of the most important aspects for this thesis will be presented.

2.1.1 Electromotive Force

The term electromotive force, usually abbreviated *emf*, was introduced in the early 1800s to described the force that would move the current through a conductor in a closed loop. This can come from a number of sources, but for the scope of this thesis, it is only discussed in terms of galvanic cells. For galvanic cells, Faraday postulated that the chemical reactions happening at the electrodes is the 'seat of the emf', i.e. these reactions drive the current. Although the term electromotive force does not coincide with the modern usage of the word force, the term is still in use to describe the cell potential, E, of a battery. This is measured in volts (V) which in SI-units are Joule/Coloumb.

If the total reaction happening in an electrochemical cell happens with negative ΔG ($-\Delta G$), it is termed a galvanic cell and the corresponding emf of that reaction would be;

$$E = \frac{-\Delta G}{zF} \tag{2.1}$$

where z is the charge transferred in each reaction and the product zF is the total charge, in coloumb, produced per mol.

As the reader knows a chemical reaction might also exhibit positive ΔG. Using the formula above it is easily seen that the corresponding emf is negative. This means that a voltage needs to be applied in order to catalyze the reaction. Such a cell is called an electrolytic cell. Most reactions are reversible, but only some, such as the ones employed in lead-acid batteries, are reversible at the operating conditions of a given cell. These cells gives a positive emf when withdrawing current (discharge) and they can be charged by applying a negative voltage, catalyzing the opposite reaction.

2.1.2 Electrode Potential

In a an electrochemical cell, the total reaction can always be divided to at least two reactions, one happening at the positive electrode, the cathode, and one happening at the negative electrode, the anode. By convention, these reactions are always written as reduction reactions and with each of these reaction a corresponding electrode potential is associated. The electrode potential measured is not an absolute quantity, but is always measured relative to a reference electrode, the most usual being the standard hydrogen electrode, $\mathrm{H^+/\frac{1}{2}\,H_2}$, commonly referred to as SHE.

For example for lithum $\mathrm{Li^+/Li}$ we have the reaction

$$\mathrm{Li^+ + e^- \longrightarrow Li(s)} \tag{2.2}$$

where the electrode potential, E, at standard conditions is -3.00 V vs. SHE [3]. If $\mathrm{Li^+/Li}$ itself was used as a reference, the electrode potential of this reaction would by definition be 0.0 V. For all reactions in this thesis that does not explicitly mention a reference, the SHE is used.

For most reactions a clearly defined standard electrode potential, $\mathrm{E^0}$ has been defined. The actual electrode potential of a reaction usually differs from $\mathrm{E^0}$, and there are several factors influencing this, such as; concentration, solvent and temperature. These factors are in literature summed up into what is called activity, a and the corresponding electrode potential is

$$\mathrm{E} = \mathrm{E^0} + (\frac{RT}{zF})\ln\frac{a_{ox}}{a_{red}} \tag{2.3}$$

where $\mathrm{a_{ox}}$ and $\mathrm{a_{red}}$ denotes the activity of the oxidized and reduced species, respectively. The experiments in this thesis are not done at standard conditions, but the electrode potentials will be close as a change in the ratio ${}^{a_{ox}}/_{a_{red}}$ by a factor of ten leads to a change of ${}^{0.059}/_{z}$ in E.

The total emf at zero current, also called the open circuit potential (OCP) of a galvanic cell would then be

$$E = E_{ox} - E_{red} \tag{2.4}$$

where $\mathrm{E_{ox}}$ and $\mathrm{E_{red}}$ denotes the electrode potential of the anode and the cathode respectively.

In this thesis the activity of a given specie will not be discussed as only electrode potentials of clearly defined systems are under investigation. It is also worth noting that the measured electrode potentials in this thesis are not directly comparable to the standard table of electrode potentials, as that table in general assumes aqueous solutions, and this is not the case for the experiments in this thesis.

2.1.3 Energy Storage

The energy of a galvanic cell is stored by having two reactants separated by a media with very low electronic conductivity and high ionic conductivity. The energy will not be released before an electronic pathway is created between the reactants completing the circuit. A general outline of a galvanic cell is shown in Figure 2.1.

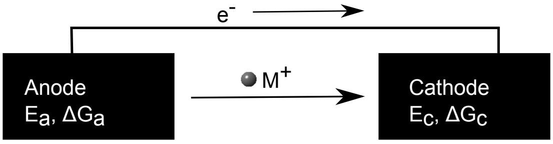

Figure 2.1: A general outline of a galvanic cell. $\Delta G_c < \Delta G_a$ and followingly $E_c > E_a$. The total cell potential of this cell is $E = E_c - E_a$. The electrons releases the chemical energy of the reaction as electrical work in the external circuit.

The total charge that can be stored is directly dependent on the amount of electroactive material in the battery.

2.1.4 Charge Transfer and Overpotential

On paper, the reactions taking place at the electrode that give rise to the electrode potential seems very simple. In reality, these reactions are the combination of a series of other reactions, such as the transport through the electrolyte, the desolvation of the ion, diffusion of the ion to the electrode surface and possibly diffusion through the electrode. Each of these part-reactions will add some resistance to the overall reaction and in order to overcome this resistance an additional force will need to be applied in the form of higher potential. This is called the overpotential[1] of an electrochemical reaction, is usually denoted η and is defined with the following relation [7]:

$$E(i) = E^{rev} + \eta(i) \tag{2.5}$$

It is important to note that η and E are functions of the current density, while E^{rev} is the reversible potential at $i = 0$. For many systems $\eta(i)$ can be approximated as a linear function of i and we get the following relation:

$$E(i) = E^{rev} + k \cdot i \tag{2.6}$$

where $\eta(i) = k \cdot i$ and k is a constant. Because the overpotential is a voltage, k can then be approximated as the internal resistance of a battery by using Ohm's law, $U = R \cdot I$.

---

[1] It could be argued that the correct technical term for this is 'polarization', but these two terms are often used interchangibly, and for a system with E^{rev} close to E^{corr} this distinction is not necessary.

For a galvanic cell this overpotential will reduce the overall voltage output and for an electrolytic cell it will increase the voltage needed to catalyze the reaction. In terms of a reversible cell the overpotential is usually divided into a cathodic (η_c) and an anodic (η_a) overpotential. The anodic overpotential is the overpotential experienced during discharge and the cathodic overpotential is the overpotential experienced during charge. The magnitude of these overpotentials may or may not be similar, depending on the nature of the reaction.

2.2 Cyclic Voltammetry

In order to characterize the electronic behavior of these materials, cyclic voltammetry was chosen as the preffered investigation method. David K. Gosser, Jr. explains in the preface of his book *Cyclic Voltammetry* [8]:

"Cyclic voltammetry (CV) has been in the forefront of the study of electron transfer and its consequences. With the cyclic voltammetric method one can simultaneously activate molecules and probe subsequent chemical reactions. The cyclic voltammetric response curve thus provides information about electron transfer kinetics and thermodynamics as well as the consequences of electron transfer"

Cyclic voltammetry is often utilized to study the reaction happening to a redox-couple in proximity of the electrode (reduction or oxidation) by recording the current response as a function of a rapidly changing potential. The information obtained from this curve can be used to extract information about the controlling processes of the reaction (diffusion, chemical reaction or electron transfer) and the number of electrons associated with the reduction/oxidation. These experiments also give information about the change in Gibbs free energy, Δ, for the reaction as this is related to the electrochemical potential, E. Information can also be extracted about the reversibility of the electrochemical reaction.

In order to study these phenomena, a three-electrode setup is commonly used such as the one shown in Figure 2.2 with one working electrode (WE), one counter electrode (CE) and one reference electrode (REF). The reference electrode is made from a material with a known reduction potential so the results obtained can be related to other potentials. A two-electrode setup is also used sometimes where the REF and CE are actually the same electrode as this simplifies the cell construction. In such a system, E^{rev} will always be close to zero, as the reversible reaction used to determine the cell potential is the same as the one being measured. The experiment is set up by suspending the reduced and oxidized species of the redox couple in an electrolyte.

The voltage is then scanned linearly across the potential-range of interest at a predetermined scan speed, measured in volts/second (V/s). The current-response from the applied potential is then recorded and presented in a current-voltage graph. Figure 2.3a, Figure 2.3a and Figure 2.3a illustrates this. Different scan speeds are used depending on the information to be extracted. For the study of a redox-couple in solution, such as $Fe(CN)_6^{3-}/Fe(CN)_6^{4-}$ a high scan speed of over 500 mV/s might be used. In the other end of the scale are the study of the diffusion of lithium into graphite which dictates a speed in the range of 15 µV/s.

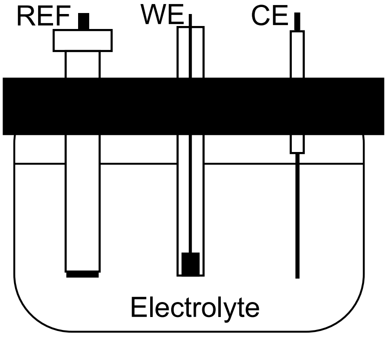

Figure 2.2: Schematics of a standard electrochemical cell used in CV-experiments.

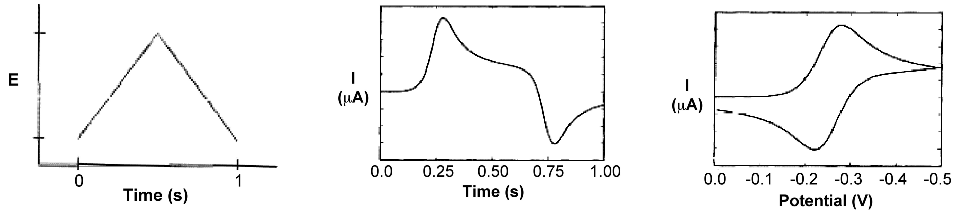

(a) Typical triangle wave applied potential.

(b) The current response over time from the applied potential in Figure 2.3a.

(c) The current in Figure 2.3b redrawn as a function of the applied potential.

Figure 2.3: Typical CV experiments on a $Fe(CN)_6^{3-}/Fe(CN)_6^{4-}$ redox couple in water. Adapted from [8].

In addition to serving as a measure for relating the applied potential to other electrode potentials, the reference electrode is also used to determine the magnitude of the applied potential. Even though the potential is always applied between the CE and WE, the potential of the CE and REF may differ significantly even if the REF and CE are made from the same material because of reaction kinetics. This is usually only an effect at high scan rates, and at lower scan rates, the potential of the two are usually similar and a dedicated reference can be omitted.

2.2.1 Extracting Data

The data extracted from the cyclic voltammograms in this study is: (1) the overpotentials; (2) the total charge transferred; (3) the reversibility of the reaction and; (4) the resistance of the cell.

Figure 2.4 shows cycle 6 of a pure magnesium electrode cycled against copper. The results of this experiment will be presented in chapter 4, but it is included here for illustrative purposes. The potential of the working electrode (E_{we}) is cycled from 0 V to -0.7 V to 1.7 V and back to 0 V. The overpotentials are calculated with the reversible potential (E^{rev}) as reference and they are indicated on the x-axis. The current levels the overpotentials are calculated from are exaggerated in this figure.

The cathodic charge (Q_c) is the amount of deposited Mg on copper and is the integral of the blue shaded area. The reverse deposition back from copper to magnesium is called the anodic charge (Q_a) and is the integral of the red shaded area. The coloumbic efficiency is calculated by dividing these numbers. The slope of graph is used to calculate the internal resistance of the battery using Equation 2.7. The important lesson here is the steeper the slope, the lower the resistance.

$$R_i = \frac{\Delta V}{\Delta I} \tag{2.7}$$

It is important to note that the overpotentials presented in this thesis is the overpotential at pre-defined, low current level, giving us the voltage where the activation energy is overcome for the reaction. The resistance presented is the slope of $E(i)$ in Equation 2.5, at higher current densities. Because the extra energy needed always is a positive ΔG, the overpotentials are always negative. However, the anodic overpotentials presented in this thesis are given as positive numbers for clarity.

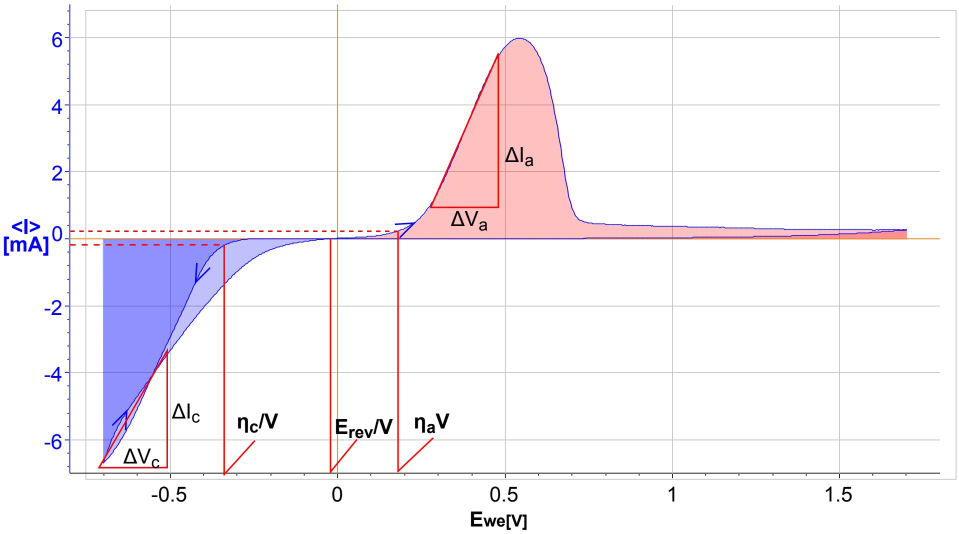

Figure 2.4: Illustration of data extracted from a CV of pure Mg vs. Cu. For explanation see text.

2.3 Battery Theory

A battery, in general terms, refers to one or more electrochemical cells that can store chemical energy and release it as electrical energy. They are divided into two types; primary and secondary batteries. Primary batteries are generally known as disposable batteries, meaning that they are based on a non-reversible electrochemical reaction and they need to be replaced after one discharge. These types of batteries include batteries such as the very common alkaline batteries and the more speculative zinc/air batteries. Secondary batteries are however constructed from reversible cells and are often also called rechargeable batteries. Common types of secondary batteries include lithium-ion, lead-acid and nickel-metal hydride batteries.

2.4 Lithium Batteries

Even though the emphasis of this report is on magnesium batteries, the general workings of a lithium-ion battery will first be given as this serves as a good basis for the understanding of rechargeable ion-transfer batteries.

A typical lithium-ion cell is shown in Figure 2.5 and contains three basic elements: the anode, the cathode and the electrolyte. In most modern batteries a porous membrane is also present between the anode and the cathode to eliminate the possibility of electronic short-circuit, minimize the electrolyte usage and increase the structural integrity of the batteries. The anode and cathode are the negative and positive electrodes, respectively, meaning that upon discharge, electrons and cations flow from the anode to the cathode. Connecting the electrodes to the complete circuit is what is collectively called current collectors.

A Li-ion battery is a so-called structural, or ion-transfer battery, meaning that the electrodes are structures that allow the ions to flow in and out of the electrode materials in a process called intercalation. When a Li-ion battery is charged, Li-ions are forced out of the cathode, through the electrolyte and onto, or into, the anode. When the Li-ions flow out of the cathode, the cathode material itself needs to be oxidized in order to accommodate the charge. So for example with a $LiCoO_2$-cathode, for every Li-ion that leaves the structure, one Co-ion has to be oxidized from +III to +IV. This happens at an approximate electrode potential of +1 V.

In the other end, at the anode, the Li-ions are reduced to Li-atoms. If the anode is pure lithium metal, this happens at the electrode potential of Li^+/Li, -3 V. If the more commonly used graphite anode is employed, the reduction happens at a slightly higher potential, between -2.7 V and -2.9 V.

When charging, because of the overpotential, the overall applied potential needs to be higher than the combined voltage needed for reducing the Li-ions and oxidizing the cathode material. So for example, a standard cell with a $LiCoO_2$-cathode

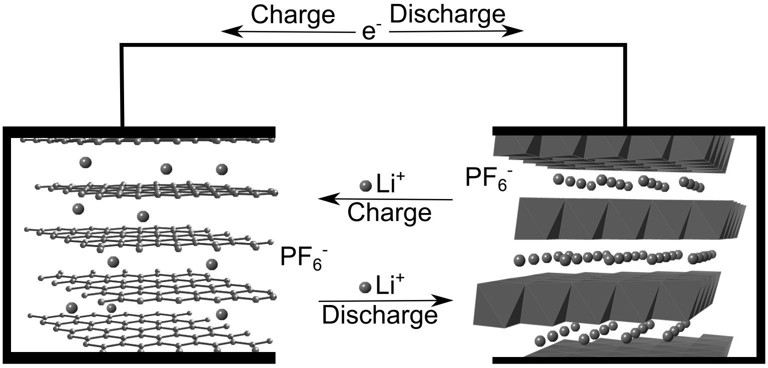

Figure 2.5: Schematic of a general lithium-ion battery cell with $LiCo_2$ cathode, LiC_6 anode and $LiPF_6$ electrolyte salt. The black boxes around the electrode materials are current collectors. The electrons in the external circuit is driven by a voltage source on charge and performs work on discharge.

and a graphite anode would have, using Equation 2.4, an approximate voltage of $1\ V - -2.8\ V = 3.8\ V$. This potential are of course influenced by several factors such as the electrolyte but also more importantly, the state of charge (SOC).

The last ions removed from the cathode requires much more energy than the first ions and followingly the oxidation voltage increases. Also, as the carbon becomes more intercalated the reduction potential of Li-ions in graphite drops towards the electrode potential of Li^+/Li, further increasing the overall voltage.

2.4.1 Anode Materials

Anode materials are the materials storing the reduced lithium atoms. Several factors affect the performance of the electrode but the most important are: (1) the voltage at which it stores the lithium; (2) the kinetics of electron transfer; (3) the ability to store lithium; (4) the available surface area; and (5) the structural integrity of the material. While (1) is a purely intrinsic material property, (2) and (3) are to some degree modifiable by different electrolytes and additives. (4) and (5) are to some extent given by the material, but they are easily modifiable. In the following sections the reference potential is Li^+/Li.

2.4.1.1 Metal

The most obvious choice for an anode in Li^+/Li system is pure lithium metal. This is the material with the highest density of lithium atoms an its reduction potential versus Li^+/Li is by definition 0 V. The general oxidation reaction for the lithium metal anode is shown in Equation 2.8.

$$\mathrm{Li^{+}(sol) + e^{-} + Li(s) \longrightarrow Li(s), E^{0}} \equiv 0\ V \tag{2.8}$$

The use of pure lithium metal in consumer products has been limited. Because the best electrolytes for a lithium ion battery creates a SEI-layer on the electrodes the redeposition of lithium is inherently difficult. It has been shown that the redeposited lithium grows dendritic structures that eventually lead to short-circuiting and danger of explosion [9]. These structures are created from uneven redeposition on the metal. When cycling, the raised structures of the metal will have higher current density than the lower parts, meaning that more metal will be deposited on the raised structures. This is then a self-reinforcing mechanism, favoring the growth of the dendritic structures. Its reactivity towards water and air is also very high making it a dangerous material to employ in consumer products.

2.4.1.2 Graphite

The most popular anode material by far is carbon in the form of graphite. The average reduction potential for $\mathrm{Li^{+}}$ in graphite is between 50 and 250 mV versus $\mathrm{Li^{+}/Li}$. This slightly reduces the overall battery voltage, which in turn reduces the energy and power output, but the cyclability and stability of these anodes is far superior to lithium metal anodes which outweighs the drawback of the voltage reduction. The general equation is shown in Equation 2.9 where (C) denotes a carbon electrode.

$$\mathrm{Li^{+}(sol) + e^{-} + (C)(s) \longrightarrow Li(C)(s), E^{0}} \approx 0.15\ V \tag{2.9}$$

The charging of these materials, is based on intercalation which means that the material does not alloy with lithium, but only stores lithium atoms between the graphene sheets. Upon lithiation, lithium atoms are inserted between ABAB-stacked graphene sheets, changing the structure to AAAA-stacking [10], see Figure 2.6. These changes are fully reversible and it has been shown that the decomposed electrolyte on cycled carbon can be washed off to make the carbon fully regain it's cycling capacity [11].

The fully lithiated anode usually is denoted with the formula $\mathrm{LiC_6}$ storing one lithium atom per six carbon atoms, giving us a theoretical gravimetric capacity of 372 mAh/g.

2.4.2 Electrolytes

The electrolyte consist of two parts, the solvent and the lithium-containing salt.

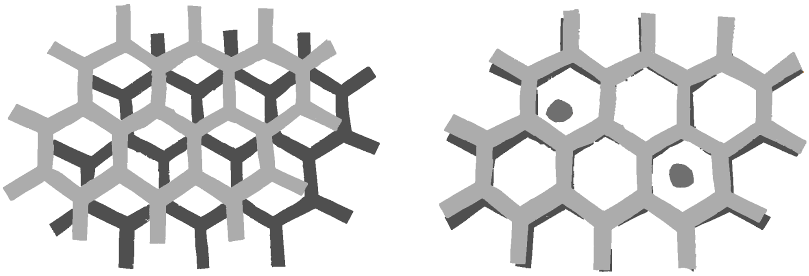

(a) ABAB-stacking of graphite before lithitation.

(b) AAAA-stacking of graphite after lithitation.

Figure 2.6: The structural changes upon lithiation of graphite.

2.4.2.1 Salt

Three main factors determines the choice of salt, namely the conductivity, the chemical and thermal stability and the toxicity. To get high conductivity it is important that the salt dissociates and dissolves completely and that the solvated ions, especially the lithium cations, have high mobility. Multiple electrolyte salts are available for use in lithium ion batteries, among others, $LiBF_4$, $LiClO_4$, $LiAsF_6$ and $LiPF_6$. The latter salt is the one employed in nearly all commercial lithium ion batteries as it is considered the best compromise between the mentioned factors [12].

2.4.2.2 Solvent

As lithium and the lithium salts are highly reactive towards water, an organic solvent has to be used and as with salts, several factors determines the choice of solvent. The primary selecting factor is that it needs to be polar in order to dissolve sufficient amounts of lithium salts, which leaves organic compounds with either carbonyl groups, nitrile groups, sulfonyl groups or ether-linkages for consideration. It should also exhibit high stability, both thermally and electrochemically, and as lithium-ion batteries often operate at voltage differences of up to 4.5 V it needs a high breakdown voltage. Finally, the composition of the solvent also determines the composition of the SEI-layer (section 2.4.3).

Ethylene carbonate (EC) was considered for the first time as a battery cosolvent by Elliot in 1964 [12] because of it's low viscosity and high dielectric constant (higher than water). It was deemed unusable for the purpose due to it's high melting point (36 °C) until the early 1970s when it was found that a co-solute would lower the melting point and after Sony's initial launch of lithium-ion batteries in 1993, it was found that mixing EC with a linear carbonate would provide the required electrochemical and temperature window [12]. Diethyl carbonate (DEC) has proved a good match and most batteries uses a 1:1 or a 3:7 mixture of EC:DEC as the solvent. Their key properties are listed in Table 2.1.

Table 2.1: Key properties of commonly used solvents in lithium-ion batteries. All data from [12].

Solvent	Structure	M. Wt	T_m [C]	T_c [C]	η [cP]	ϵ	ρ (25 °C) [gcm^{-3}]
EC	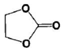	88	36.4	248	1.90 (40 °C)	89.78	1.321
DEC	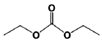	118	-74.3	126	0.75 (25°C)	3.107	1.063

2.4.3 SEI-layer

It is known that lithium metal anodes reacts with both liquid and polymer electrolytes and is covered by a passivating film that slows the corrosion of lithium and the decomposition of the electrolyte. This film serves as an interface between the anode and the electrolyte and is therefore named solid electrolyte interface, or SEI. Because the film is electronically non conductive and electrons are needed for the decomposition and deposition of the SEI, the SEI-thickness is limited by the electron tunneling range [13]. A very simple equation for the formation of the SEI-layer is given in Equation 2.10 where (SEI) denotes the SEI-film and (EC:DEC) is the solvent. The film is conductive for lithium ions, but does have a certain resistivity, so a very thick SEI-layer will increase the cell resistance.

$$\mathrm{Li^+(sol) + e^- + (EC{:}DEC)(l) + LiPF_6(sol) \longrightarrow Li(SEI)(s), E^0} \approx 0.7\ V \qquad (2.10)$$

In ordinary lithium-ion cells the SEI-film is formed on the anode during the first charge, whether it is lithium metal or carbon, when lithium ions first are forced towards the anode.

The chemistry of the formation of the SEI-layer is intrinsically complex and not very well understood. The composition is also not completely known but it generally consist of decomposed electrolyte, both solvent and salt. For example Verma et al. [14] lists that among other chemicals the SEI-layer contains $LiPF_6$, LiF, Li_2O, Li_2CO_3, $(CH_2OCO_2Li)_2$ and $ROCO_2Li$.

2.4.4 Cathode Materials

Cathodes in a secondary lithium-ion batteries are so-called intercalation cathodes. Whereas regular carbon anodes also are intercalation electrodes, they merely store the lithium as atoms close to the voltage of the Li/Li^+ electrode potential. Cathode materials, on the other hand, are crystal structures with lithium as one of the major constituting elements. The key factors for cathode materials are high ionic conductivity of lithium, high electronic conductivity, favorable volume expansion upon discharge, high energy density and being able to accommodate the extra charge and tension left in the structure when lithium ions are removed from the structure.

A general chemical equation for the charge reaction of a cathode is as follows:

$$\mathrm{LiMO(s)} \longrightarrow \mathrm{Li^{+}(sol)} + \mathrm{MO(s)} + \mathrm{e^{-}} \tag{2.11}$$

where MO denontes a metal oxide. As one can see, high ionic and electronic conductivity of the cathode are of great importance for the charge rate. For every lithium ion de-intercalated from the structure, an electron has to travel from the cathode material to the current collector to complete the charge balance. This has huge implications as many of the best cathode materials are very poor electronic conductors. In most commercial batteries, the electronic conductivity is increased by adding small amounts of an electrical conductor, such as carbon black, to the cathodes.

When lithium ions are deintercalated from the cathode structure the internal stress in the structure increases for a two reasons. First, in order to balance the charge, the remaining ions have to be oxidized, changing the extent of the electron orbitals of these ions. And secondly the space previously occupied by a lithium ion, now represents a defect, for which the structure itself has to compensate for.

Table 2.2: Typical lithium-ion cathode materials. Data from [15].

Material	Voltage vs. $\mathrm{Li}/\mathrm{Li}^{+}$	Theoretical Capacity	Usable Capacity
$LiCO_2$	4.3 V	273.8 mAh/g	160 mAh/g
$LiNiO_2$	4.3 V	274.4 mAh/g	220 mAh/g
$LiFePO_2$	4.0 V	169.9 mAh/g	160 mAh/g
$LiMn_2O_4$	3.5 V	148.3 mAh/g	110 mAh/g

2.5 Magnesium Batteries

2.5.1 Theory

The key atomic properties of magnesium (Mg) are listed in Table 2.3.

Atom number	12
Atomic weight	24.3050 u
Atomic radius	150 pm [16]
Ionic charge	+2
Ionic radius	86 pm [4]

Table 2.3: Key properties of magnesium

As mentioned in the introduction the reasons for using magnesium as a basis for a battery are: (1) the relatively high negative reduction potential; (2) the relatively low atomic weight; (3) the abundance and; (4) the fact that it is divalent. The standard electrode potential of magnesium reduction is -2.367 V which is high compared to zinc (used in alkaline batteries) but somewhat lower than the reduction potential of lithium.

One magnesium atom weighs almost four times as much as one lithium atom (6.9 u), but as a potential battery-consituent this is somewhat outweighed by the fact that it is divalent, i.e. the Mg-ions carries twice the charge of a Li-ion. The abundance of magnesium is also indisputable, in fact, magnesium is the second most abundant element in the mantle with the mantle consisting of 38 wt% MgO [17]. The crust of the earth however contains 3.5 wt% magnesium, still several orders of magnitude more than lithium at 10µg/g [5].

While the theoretical gravimetric charge density of magnesium is lower than that of pure lithium (2233 mAh/g vs. 3884 mAh/g) the theoretical volumetric charge density is almost the double that of lithium (3881 mAh/cm^3 vs. 2074mAh/cm^3). This means that while magnesium batteries might be heavier, they will be smaller.

Pure magnesium is in a hexagonal close packed (HCP) structure and, as a metal, it offers specific strength comparable to that of aluminum but with limited ductility.

However, the divalency of magnesium comes at a cost; because of this it has very limited conductivity in most solid structures. This also happens to include SEI-layers and therefore, any electrolytes breaking down to form a SEI-layer on the electrode surface is rendered useless. In addition it is very hard to find good cathode materials as the Mg-ions are immobile in structures similar to cathode materials for lithium-ion batteries. This is also the reason why magnesium can not be intercalated into graphite.

2.5.2 Electrode Materials

2.5.2.1 Metal Electrodes

In all articles discussing the potential of secondary magnesium batteries, pure magnesium is used as the anode material. Of all theoretical materials, it has the highest gravimetric charge density since it only consist of magnesium atoms.

It's relatively high reduction potential also means that it easily reacts with other materials and forms magnesium oxide when brought into contact with air, and especially moist air. What further complicates the use of magnesium is the fact that the magnesium oxide has a much higher density than pure magnesium, and the oxide layer formed is thus porous and does not protect the underlying magnesium from further oxidation [18].

Most magnesium materials, however, offer a reasonable corrosion resistance in the normal atmosphere, but it is believed that this is due to impurities rather than the inherent properties of magnesium [19].

Alloying magnesium improves the corrosion resistance, the ductility and other mechanical properties of the metal. The mechanical properties of magnesium alloys are beyond the scope of this thesis, but these alloys are significantly cheaper than pure magnesium and the focus will be on the electrochemical behavior of four, cheap and commercially available alloys. These alloys are alloyed with aluminum, tin, zinc and lead and trace amounts of manganese. It is thought that the electrochemical behavior of these alloys would not be too far from pure magnesium, as magnesium has the most negative reduction potential of these elements and therefore would be the metal transporting most of the current.

It is expected that the same problems with dendritic structures, mentioned in section 2.4.1.1, will affect magnesium metal electrodes, but to a lesser degree as the electrolytes does not decompose to form a passivating layer on the electrode surface.

2.5.2.2 Intercalation Electrodes

The biggest obstacle towards commercialization of magnesium ion-transfer batteries is the lack of suitable cathode materials. Levi et al. wrote in 2010 an excellent article summing up the challenges and pathways for new cathode materials in the future [20]. It concludes that new cathode materials are needed, but even though they're not excellent, there exist a few working cathode materials for magnesium ion-transfer batteries. These are open-framework structures that is not made from magnesium itself, but into which magnesium can be intercalated. A summary of the two structures showing some promise are given below.

$Mg_xV_2O_5$ Vanadium (V) oxide (V_2O_5) and the hydrated vanadium bronzes ($MeV_3O_8(H_2O)_y$, Me = Li, Na, K, $Ca_{0.5}$ $Mg_{0.5}$) were studied as possible magnesium intercalation hosts as early as 1993 [21, 22]. They showed high initial charge densities, upwards of 200 mAh/g, but this decreased rapidly with cycling before stabilizing around 80 mAh/g. However, it was found that for the increased layer separation and the high charge density, water in the bronzes were of key importance and this renders the materials mostly unusable with most popular electrolytes.

Later improvements have improved the energy density and reliability of vanadium oxide as cathode material, and Inamura et al. was able to make a cathode of this material with a voltage of -0.8-0.4 v vs. Ag^+/Ag [23]. This translates to a possible magnesium-ion battery with a total cell voltage of over 2 V. Other research includes vanadium oxide nanotubes [24].

$Mg_xMo_3S_4$ Mo_3S_4 was first synthesized by Chevrel et al. [25] in 1974 and is therefore called a Chevrel-type compound. It is a very open network-structure with 'canals' and Chevrel et al. suggested that most small cations can form the phase $Me_xMo_3S_4$ (Me = Cu, Ni, Co, Fe, Mn, Cr, Mg, Cd, Zn), with $0 < x < 1$. They were however only able to synthesize the $M_xMo_3S_4$ with Me = Al, Cu, Ni, Co and Fe.

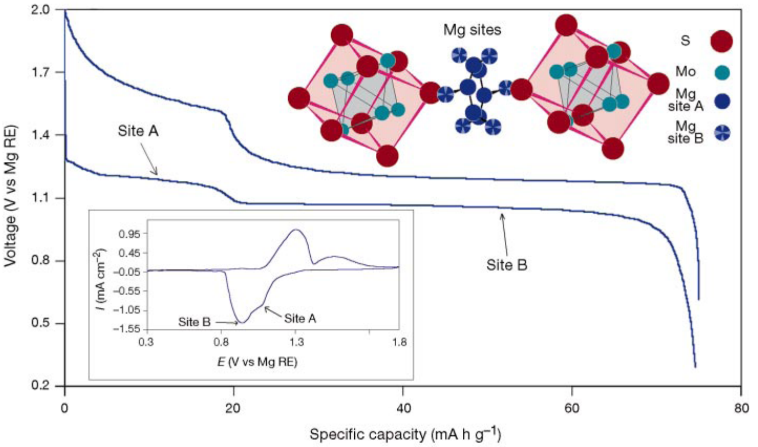

Figure 2.7: Typical electrochemical behavior and the basic structure of $Mg_xMo_3S_4$, $0 < x < 1$. Main figure: A chronopotentiogram taken with a constant current of 0.3 mA cm-2. Inset: A cyclic voltammogram taken with 0.05 mV/s. Adapted from [26]

It was investigated as an magnesium electrode in 2000 by Arubach et al. [26], where they synthesized $CuMo_3S_4$ and removed the copper either chemically with $FeCl_3$ or electrochemically. It was then cycled against pure magnesium metal and as a magnesium intercalation electrode the $MgMo_3S_4$ has a theoretical charge density of 121.8 mAh/g. They were however only able to achieve a practical charge density of 80-100 mAh/g, but with an excellent cyclability of over 2 000 cycles without more than 15% capacity fade. The electrode potential of this material is 1-1.3 V vs. Mg^+/Mg.

2.5.3 Electrolytes

While lithium electrolytes are chosen to make create an SEI-layer of decomposed electrolyte at the electrodes, magnesium electrodes needs to be kept bare. This is due to the fact that the conductivity of magnesium is very low in these thin films.

2.5.3.1 Solvent

Because magnesium is rapidly covered by a passivating film of MgO when brought in contact with water or other protic solvents, only aprotic solvents can be used [27]. Two such solvents are diethyl ether and tetrahydrofuran (THF), with the latter being the far most used in research and development of secondary magnesium batteries. THF was chosen for this thesis because of its lower volatility, lower toxicity, higher availability and its established role in similar research.

Table 2.4: Key properties of the solvents used in the study. All data from [28].

Solvent	Structure	M. Wt	T_m [C]	T_c [C]	η [cP]	ϵ	ρ [gcm^{-3}]
THF	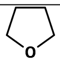	72.11	-108	65	0.46 (25 °C)	7.52 (22 °C)	0.889
Diethyl ether	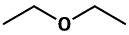	74.12	-116.3	34.6	0.224 (25 °C)	4.26 (20 °C)	0.713

2.5.3.2 Salt

Due to the aprotic limitation of solvents for magnesium batteries, only a handful of electrolyte salts are available. These aprotic solvents are not very good solvents for regular salts as they have very dielectric constants and it has been shown that dissolution and deposition of Mg from simple salts, such as $MgCl_2$ and $Mg(ClO_4)_2$ in aprotic solvents, is not possible[29].

The first research on magnesium for battery purposes was done with so-called grignard reagents. These are organomagnesium complexes on the form RMgX where X is a halogen and R is an alkyl group such as methyl (Me), ethyl (Et), butyl (Bu) or phenyl (Ph). These are readily available as commercial solutions of the given grignard reagents in THF.

In 2002 Aurbach et al. did a thorough study on different organomagnesium chloroaluminate complexes for reversible magnesium dissolution and deposition [29]. They combined Lewis bases on the form R_2Mg with Lewis acids on the form $AX_{3\text{-}n}R'_n$, where R and R' are alkyl groups, X is a halogen and A is an element forming +3-cations such as boron or aluminum. In total they studied 22 different combinations of Lewis acids and Lewis bases.

The best electrolytes in this group offered superior cycling efficiency, close to 100%, and increased electrolyte decomposition voltage when compared to grignard reagents. The first electrolyte of this thesis was therefore chosen as a 0.25M $Bu_2Mg\text{-}AlCl_3$ combination in a 1:2 ratio in THF, commonly denoted using the stochiometric formula $(BuAlCl_3)_2Mg$. This was measured in the previous mentioned article to have a cycling efficiency of around 75% and an electrolyte decomposition voltage of 2.4 V.

In 2007 Mizrahi et al. published an article using another combination of Lewis acids and bases with even better properties in terms of cycling efficiency and electrolyte decomposition voltage. This complex, termed the 'all phenyl complex' (APC), consist of the Lewis base PhMgCl and the Lewis acid $AlCl_3$ in a 2:1 ratio in THF. This electrolyte offers a near 100% cycling efficiency and an electolyte decomposition voltage of 3 V. In solution the anions are described as $AlPh_4^-$ and $AlPh_{4\text{-}n}Cl_n^-$ (n = 1-3) and cations of the type $MgCl^+$ or $Mg_2Cl_3^+$. The greater stability is attributed to the lack of carbon-magnesium bonds with the aluminium-carbon bonds being more electrochemically stable.

This was chosen as the second electrolyte of the study.

2.6 SEM and EDS

The scanning electron microscope (SEM) is one of the most commonly used techniques for investigating samples at the microscopic level. It works by accelerating electrons at a given acceleration voltage and focusing them into a very small spot on the sample. This spot is then raster-scanned across the surface. The electrons are then either scattered or absorbed and re-emitted. These are called back-scattered electrons (BSE) and secondary electrons (SE).

The electrons coming from the sample are then recorded by detectors in the SEM, and combined with information about where the beam is, a picture can be obtained.

Energy dispersive spectroscopy (EDS) is an instrument mounted together with the SEM. When the accelerated electrons strike the surface, some electrons in the material are removed or exited from their shells. When thse electrons relax back into their previous shell, energy is released in the form of x-rays. Because every element has its own specific orbitals, an elemental-map can be created by recording the characteristic x-rays.

When recording this map, the counts for each energy level are recorded over a given time, and the energy levels where a peak is found corresponds to a given element. EDS is a very good instrument for qualitatively detect the prescence of an element, but quantization is inherently difficult. This is because different elements have a very different beam cross-section, meaning that the number of counts recorded for two elements does not say anything about ratio between them.

3 Experimental

3.1 Chemicals

Table 3.1 lists the chemicals used in this thesis and Table 3.2 lists the alloys used and the major constituting elements of these alloys.

Table 3.1: Chemicals used in this thesis.

Material	Full name	Formula	Application area
THF	Tetrahydrofuran	$(CH_2)_4O$	Electrolyte solvent
$AlCl_3$	Aluminium chloride	$AlCl_3$	Electrolyte reagent
PhMgCl	Phenylmagnesium chloride	C_6H_5MgCl	Electrolyte reagent
Bu_2Mg	Dibutyl magnesium	$(C_2H_5)_2Mg$	Electrolyte reagent
V_2O_5	Vanadium Oxide	V_2O_5	Electrode material
Copper	Copper sheets	Cu	Cathode

The full specifications, such as purity and manufacturer, can be found in Table A.1 in Appendix A.

Table 3.2: Magnesium alloys used in this thesis. The amount of alloying elements are given in wt%.

Material	Aluminium	Zinc	Tin	Lead	Manganese	Purity
Magnesium						99.9%
AZ31	3.0	0.71			0.19	n/a
AZ61	6.2	0.61			0.22	n/a
AT61	6.0		1.0		0.01	n/a
AP65	6.3	0.6		4.7	0.18	n/a

The full specifications, such as purity and manufacturer, can be found in Table A.2 in Appendix A.

3.2 Equipment

The equipment used in this project is listed in Table 3.3. During the initialization phase of this project potentiostat 1 was used, but due to some problems it was changed and all the results presented are recorded using potentiostat 2.

Table 3.3: Equipment used during this thesis.

Equipment	Producer and model
Glove box	MBraun LABmaster sp
3-electrode cell	Hohsen HS-3E Test Cell
Coin cells	Hohsen 2016 stainless steel coin cells
Potentiostat 1	Gamry Reference 600
Potentiostat 2	Bio-logic VMP3
Thickness gauge	Mitutoyo Absolute ID-C112BS
SEM	Hitachi S-3400N

3.3 Electrolyte Preparation

3.3.1 $(BuAlCl_3)_2Mg$

This electrolyte was prepared as in ref. [24] by Silje Rodahl in the following fashion:

- 1 M Bu_2Mg in heptane was poured in a beaker and placed on a magnet stirrer
- $AlCl_3$ was added
- The mixture was stirred for 48 h while the heptane was allowed to evaporate
- THF was added to the white powder to obtain 0.25 M $(BuAlCl_3)_2Mg$

3.3.2 All Phenyl Complex

The ‘all phenyl complex’ (APC) is a mixture of the Lewis base PhMgCl and the Lewis acid $AlCl_3$ in a 2:1 ratio in THF. It was not made due to safety issues with the glove box arising just before it was supposed to be made. The procedure to make 10 ml 0.4 M $Mg_2Cl_3Ph_2AlCl_2$/THF would have been like this:

- Add 0.533 g AlCl3 to 6 ml THF
- Add 4 ml 2M PhMgCl

This is a much simpler electrolyte to make.

3.4 Electrode Preparation

3.4.1 Metal Electrodes

The magnesium and -alloys used in this thesis were ordered in sheets, 0.25 mm thick, packed in air. A special tool was designed and made for stamping out 14 mm discs to be used as electrodes in the coin cells and 3-electrode cell. Because these electrodes were exposed to air, a passivating oxide-film formed on the surface. Before the cells were assembled, the electrodes was either etched and polished or just polished.

The etching was done with chromic acid at room temperature in a fume hood. The chromic acid was prepared by dissolving chromium trioxide, CrO_3, in water at a weight ratio of 180 g/l. After being stamped out, the electrodes were etched for 2 to 5 minutes until the white layer of magnesium was gone. The electrodes were then washed in two water baths and transferred to the glove box through the vacuum chamber. All pure magnesium electrodes received this treatment and the alloy-electrodes receiving this treatment are marked with an 'e´ to denote the etching.

Polishing was done just before assembly. The pure magnesium electrodes were first polished with a cloth, to remove most of the newly formed oxide layer and then with the fine-gritted sandpaper. Before polishing, all electrodes had streaks in them from the sheet metal forming (Figure 3.1a), and the electrodes were polished perpendicular to these streaks until the streaks were no longer visible (Figure 3.1b). This ensured a total removal of the surface layer and removal of enough material to avoid most problems with a deformed surface layer.

Some electrodes received neither etching nor polishing prior to assembly. These electrodes are marked with an ‘u’, denoting untreated.

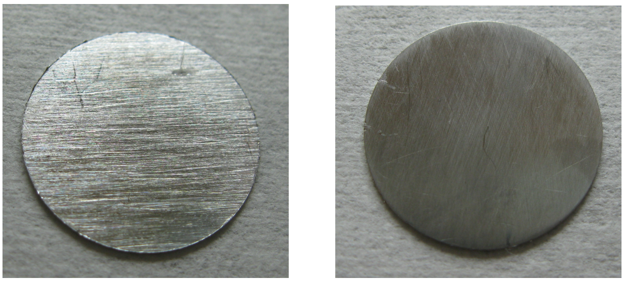

(a) AZ61 electrode before polishing

(b) AZ61 electrode after polishing

Figure 3.1: Comparison of electrodes before and after polishing

3.4.2 V_2O_5

The V_2O_5 electrodes was prepared by Silje Rodahl in the following fashion:

- 5 g V_2O_5-powder dissolved in small amounts of 50/50 aceton/water.
- 0.48 g teflon binder dissolved in small amoounts of 50/50 aceton/water
- Mixing the two
- Add 1 g of carbon black
- Stirring and addition of enough 50/50 aceton/water to form a stable suspension.

It was then tapecasted as a 15 µm film on Al-foil and dried in a vacuum-oven before transfer to the glove-box.

3.5 Cell Assembly

Everything was assembled in the glove box in an Argon atmosphere containing less than 0.1 ppm water and less than 0.1 ppm oxygen. Transferring materials and equipment into this box was done utilizing a load-lock, or antechamber.

3.5.1 3-Electrode Cell

The three-electrode cell used in the experiments is a round cell and cut-through schematics can be seen in Figure 3.2, while the dimensions of the materials are listed in Table 3.4. For the circular components, only diameter is listed.

Table 3.4: Sizes of the different cell components.

Function	Material	Size	Thickness
Working electrode	Copper	⌀14 mm	0.25 mm
Counter electrode	Mg-alloy	⌀16 mm	20 µm
Reference electrode	Magnesium	1×4 mm	0.25 mm
Separator	Polyester	⌀24 mm	20 µm

First the three electrodes were prepared. The reference electrode (REF) was made from the pure Mg-foil and together with the counter electrode (CE) of the chosen alloy they were polished as described in the previous section. A ⌀16 mm cutting tool was used to cut out a disc from the Cu-foil to act as working electrode (CE).

The cell was then assembled in the following order:

1. Separator on the WE side
2. Plastic spacer on the WE side
3. Working electrode (WE)

4. WE current collector
5. WE side enclosure
6. Two drops of electrolyte
7. Reference electrode (REF)
8. Separator on the CE side
9. Two drops of electrolyte
10. Plastic spacer on the CE side
11. Counter electrode (CE)
12. CE current collector
13. CE side enclosure

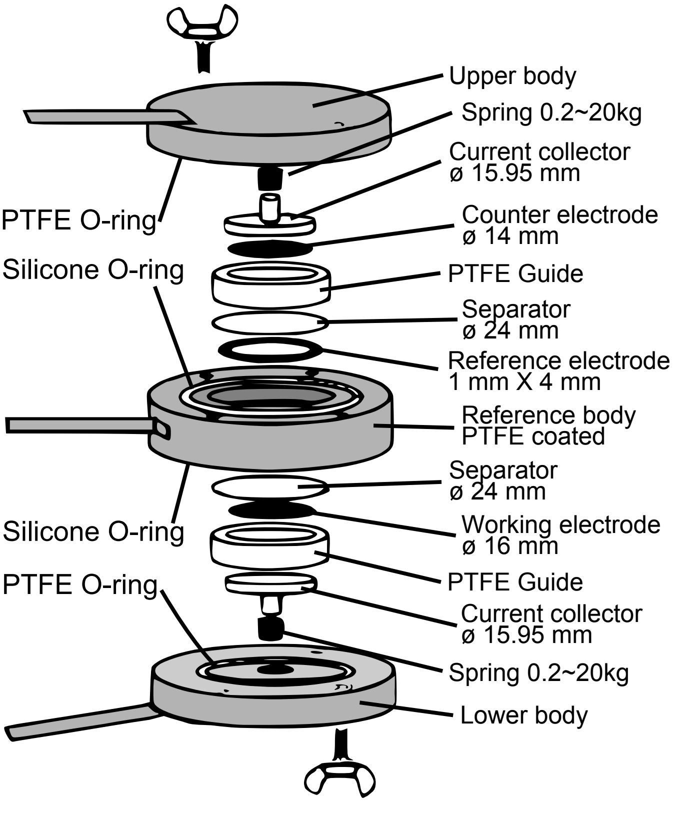
Upper body
Spring 0.2~20kg
Current collector
ø 15.95 mm
PTFE O-ring
Counter electrode
ø 14 mm
Silicone O-ring
PTFE Guide
Separator
ø 24 mm
Reference electrode
1 mm X 4 mm
Reference body
PTFE coated
Separator
ø 24 mm
Silicone O-ring
Working electrode
ø 16 mm
PTFE O-ring
PTFE Guide
Current collector
ø 15.95 mm
Spring 0.2~20kg
Lower body

Figure 3.2: Schematics of the three electrode cell used in our experiments. The drawing is made from data obtained at [30].

3.5.2 Coin Cells

The coin cells are 2016-cells, meaning that they have outside diameter of 20 mm and outside height of 1.6 mm. It uses the same dimensions of materials as listed in Table 3.4 with the exception of the separator having a diameter of 17 mm. In addition, stainless-steel spacers were inserted on the Mg-side in the coin cells, to fill up the battery cavity. Spacers of 0.6 mm and 0.8 mm were used to assess the effect of differing internal pressures. The spacer thickness is indicated after the anode material for the coin cells.

These cell was then assembled in the following order:

1. Bottom enclosure
2. Gasket
3. Spacer
4. Working electrode (WE)
5. Separator
6. Two drops of electrolyte
7. Counter electrode (CE)
8. Top enclosure

In total, 30 cells were made to distinguish the effects of internal pressure, pre-treatments and alloying elements. However due to many of these cells short-circuiting during assembly, only about 10 yielded results.

Three cells were also assembled with V_2O_5 intercalation cathodes and Mg, AZ61 and AZ61e anodes, respectively. 0.6 mm spacers were used and two drops of electrolyte were added to the cathode to soak the material before adding the separator.

3.6 Measurements

3.6.1 Initial Measurements

The first part of the measurements was carried out to obtain potential limits and scan speeds to be used in the measurements. Several experiments were done at different scan speeds, ranging from 1 mV/s to 20mV/s. Different scan-limits were also tested and after a thorough review of the results presented in section 4.2, the measurement scheme presented in the following section was established.

3.6.2 Measurement Scheme

This study is not as much concerned with the electrochemistry happening in the solution, but more concerned with the electrochemistry of the electrodes. This dictates a medium scan speed (20 mV/s). Measurements carried out at this speed is well-suited to differentiate the magnesium alloys and characterize the breakdown voltage of the electrolyte. The full measurement scheme can be seen below and in Figure 3.3.

1. 2 hours initialize - Measurement of Open Circuit Potential (OCP)
2. Linear Sweep Voltammetry (LSV) - From OCP to 0 V at a speed of 1 mV/s
3. Cyclic Voltammetry (CV) - 20 cycles From -0.7 V to 1.7 V at a speed of 20 mV/s
4. LSV - From 0 V to 4.0 V at a speed of 20mV/s

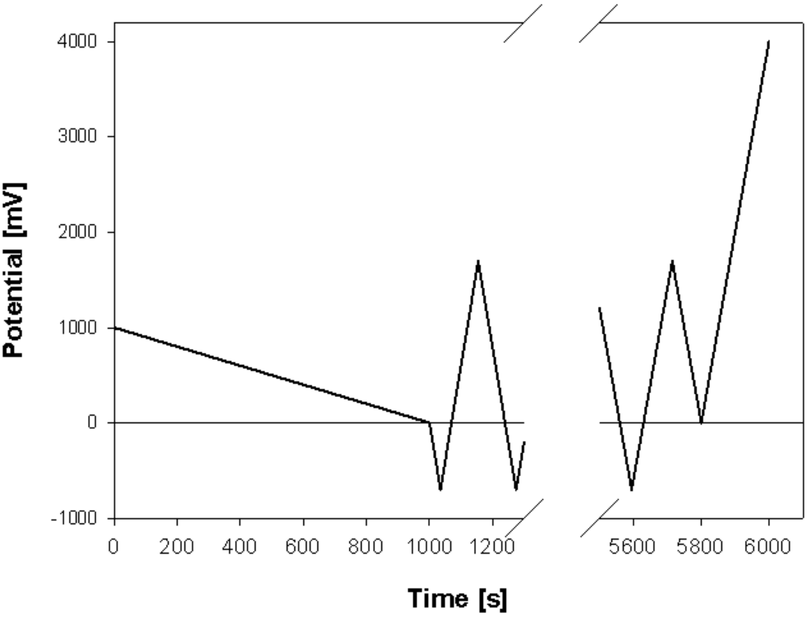

Figure 3.3: Graphic presentation of the potential applied as a function of time.

The initialization period is used to let the battery relax before applying any voltage to it. Then the voltage is slowly brought down to 0 V before starting the cycling. After the cycling the voltage is swept to 4.0 v and a current peak is expected where the electrolyte starts decomposing. The voltage was stepped in steps of 0.3 mV and the current, I, was measured and averaged over 10 potential-steps to give <I>, which is the number presented. The potentiostat used is a Bio-Logic VMP3 and the software used to collect and analyze data was Bio-Logic EC-lab. The intercalation electrodes were first cycled two cycles at 1mVY/s and then one cycle a ramp speed of 10µV/s in order to obtain data about the intercalation process.

Most batteries experienced a total failure before 20 cycles were run and therefore, the cycling of some batteries were stopped after 11 cycles to assess the anodic stability of the electrolyte.

3.7 SEM

After cycling, the cells were disassembled in the glove box. From the cells cycled towards the end, the electrodes were kept and brought into another lab for SEM-study. This happened in air and it was expected that the THF would dry off and any magnesium exposed to air would oxidize. Before the SEM, the samples were washed with 70% ethanol.

All pictures were taken with back scattered electrons at a resolution of 500X and image mode COMPO. This mode is best suited to enhance the differences at surface composed of several elements. The acceleration voltage was varied between either 5 kV or 15 kV depending on which acceleration voltage gave the best images.

EDS-spectra were recorded at an acceleration voltage of 15kV over 5 minutes.

4 Results

4.1 Measurements

This section extends the experimental section by providing details of how the data is presented. All the data such as charge (Q), efficiency (Eff) and resistance (R) are averaged over the 5 last cycles of the CV. The reversible potential (E^{rev}) is averaged over all the cycles and the overpotentials (η) are given for the first and last cycle, see section 4.1.2.

As mentioned, a total of 45 cells were assembeled, counting both batteries and 3-electrode-cells. The data from the 3-electrode cells are presented in section 4.2.2, and due to the reasons discussed in section 5.1, they are not used for charge calculations. Of the 30 batteries assembeled, only about 10 yielded results due to instrument error or cells short-circuiting during assembly.

All the currents presented in the graphs are actual currents of the assembeled cells. To obtain the current density, the current should be divided by the electrode area ($(0.7\ cm)^2\pi = 1.54\ cm^2$).

4.1.1 Cycles

When cycling the batteries, at some point most of the batteries experienced a total failure, rendering them useless. This failure was seen as high increase in current together with much more noise appearing in the cyclic voltammograms. The failure was usually seen during the plating of Mg on the copper and was very often preceded by an increased signal in the anodic area in the previous cycle. This can be seen in Figure 4.1 which is included in this section for illustrative purposes. Throughout this thesis, the number of cycles quoted for a given material is the number of charge-discharge cycles run before any noise indicating breakdown is seen. For example, the number quoted for AT61 in Figure 4.1 is 9.

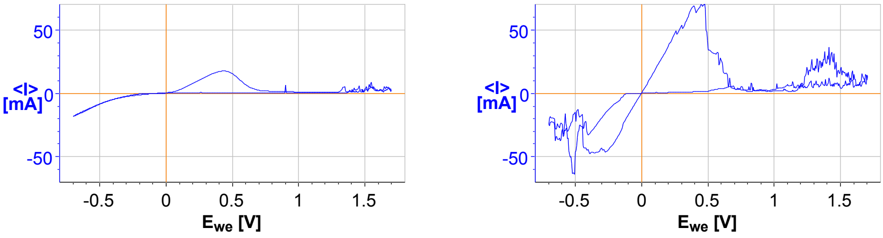

Figure 4.1: The 10th and 11th cycle of the AT61 specimen with 0.6 mm spacer.

If a battery did not experience a failure during cycling, the numbers listed are marked with a star (*).

4.1.2 E^{rev} and Overpotentials

The reversible potential of a two-electrode cell, such as coin cells should be 0 V due to the fact that the reference electrode is the same as the counter electrode. This is however not the case for most of the measurements presented in this paper and the reversible potential is calculated as the potential where the line crosses the x-axis in the scan from -0.7 V to 1.7 V, averaged over all the cycles. This potential is very stable throughout the cycles, as seen in Figure 4.2

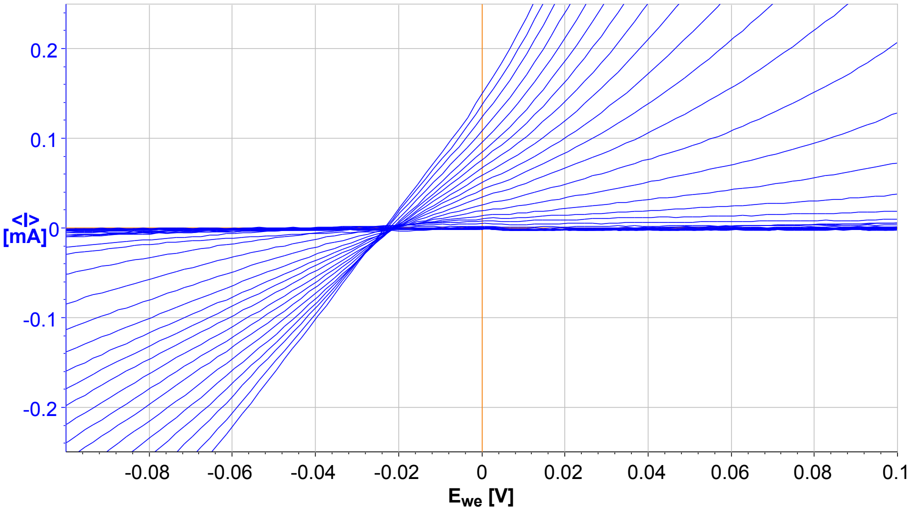

Figure 4.2: A closeup around E^{rev} of the Mg electrode shown in Figure 4.9. The spread is representable for all measurements.

The overpotentials mentioned in the following sections are defined as the additional potential that needs to be applied before the plating or redopsition starts. It is important to note that these overpotentials are for an electrochemical cell ramped at 20 mV/s and not steady-state overpotentials. To have a comparable and numeric analysis of when the reaction starts, the overpotential has been defined as the potential when the cells have a current density of 0.1 mA/cm^2.

One common trend for all the assembled cells is that the overpotential is highest at the first cycle and gradually decreases during cycling. Therefore, four overpotentials are presented for each of the materials, two anodic overpotentials (η_a), one for the first cycle and one for the last cycle, and two cathodic overpotentials (η_c) for the same cycles.

4.2 Initial Measurements

The different series of runs such as unetched vs. ethced and with varying internal pressures was originally intended to be done with all the different alloys. However, due to problems with some potentiostat-channels and many of these cells short-circuiting during assembly, results were only obtained for some of the electrodes.

4.2.1 Scan Speeds

In order to find a measurement scheme suitable for distinguishing the different alloys, several runs with different scan limits and different ramp speeds were done. The electrolyte stability windows was used to determine the scan limits. These results are presented in the data about electrolyte stability, section 4.4. Initially, scan speeds of 1 mV/s and below were used but no useful data were obtained at these speeds, However, we were able to run one Mg-electrode first 11 cycles at 20mV/s and then 3 cycles at 10mV/s before failure. The charge data for the 11th and 12th cycle of this experiment are presented in Table 4.1 with a comparison of the runs in Figure 4.3.

Table 4.1: Comparison of the 11th cycle at 20mV/s and the 12th cycle at 10mV/s for a Mg-electrode

Cycle	R_c [Ω]	R_a [Ω]	Q_c [mAh]	Q_a [mAh]	Eff [%]
11	12.5	10.52	0.09622	0.09171	95.32
12	14.3	12.1	0.1914	0.1866	97.53

4.2.2 External Reference

Some runs were also done using the three-electrode cell with magnesium as a reference to determine the electrode potential of the the alloys. The CV's were carried out on pure Mg and AZ61 and the overpotentials and reversible potentials of these are presented in Table 4.2 while the the last cycles recorded at 20 mV/s for these electrodes are shown in Figure 4.4

Table 4.2: The reversible potential and overpotentials of Mg and AZ61 with an external Mg-reference.

Material	E^{rev} [V]	$\eta_{c,1}$ [V]	$\eta_{a,1}$ [V]	$\eta_{c,last}$ [V]	$\eta_{a,last}$ [V]	Cycles
Mg	-0.23	-0.22	0.12	-0.08	-0.02	11
AZ61	-0.21	-0.41	0.36	-0.14	-0.01	21

The results of these CV's are not used for charge calculations due to reasons discussed in section 5.1.

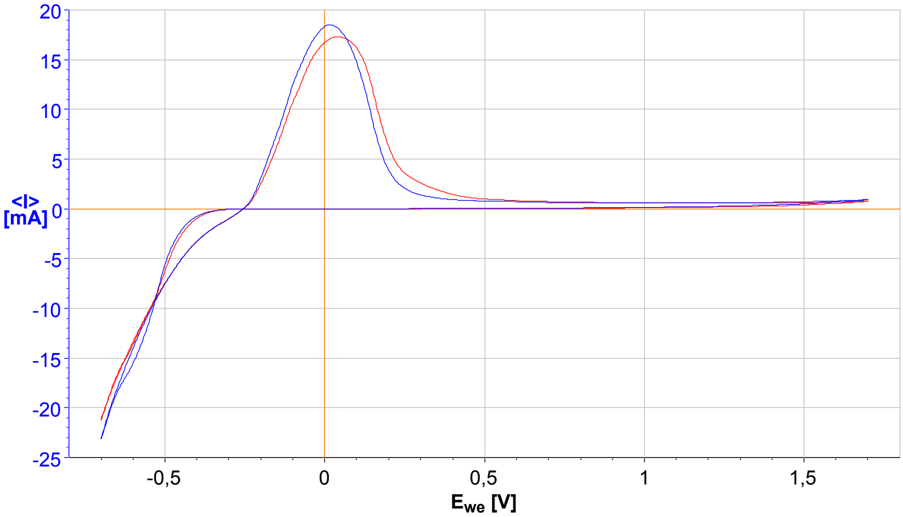

Figure 4.3: The 11th cycle of a Mg-electrode at 20mV/s (blue) and the next cycle at 10mV/s (red). The reason why the reversible potential is not 0 V is discussed in section 5.1.

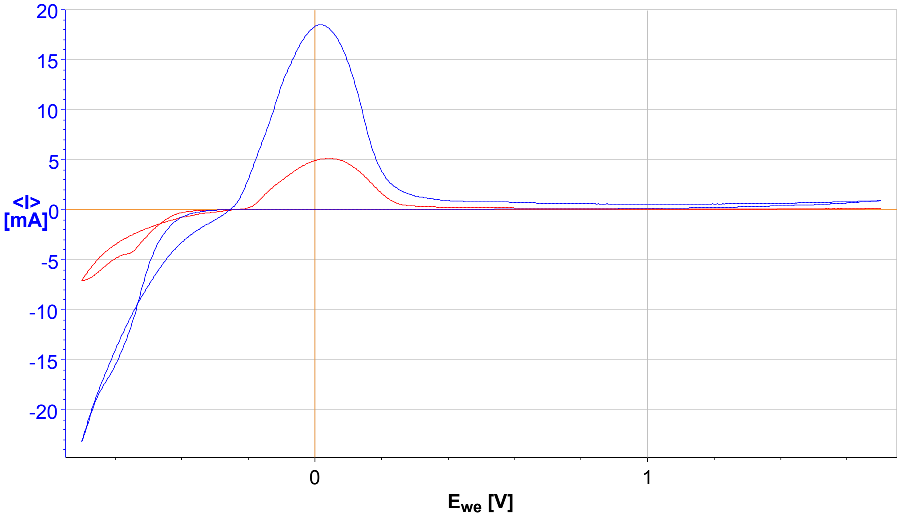

Figure 4.4: The last cycles at 20mV/s with Mg (blue) and AZ61 (red) electrodes with Mg as an external reference. This is the 11th and 21st cycle, respectively.

4.2.3 Internal Pressure

The internal pressure was, as mentioned earlier, varied by the amount of spacers used when assembling the cells. Two different thickness' were used, 0.6 mm and 0.8 mm. Complete runs from cells made with 0.6 mm spacers and 0.8 mm spacers were only obtained with AT61 and the data from these runs are presented in Table 4.3. The first and last cycle of these batteries are shown in Figure 4.5 and Figure 4.6, respectively.

Table 4.3: Comparision of the effect of internal pressure measured on batteries assembled with AT61-electrodes and 0.6 mm or 0.8 mm spacers.

Spacer	E^{rev} [V]	η_c [V]	η_a [V]	Q_c [mAh]	Q_a [mAh]	Eff [%]	Cycles
0.6 mm	-0.06	-0.1	0.04	0.07868	0.07482	94.61	9
0.8 mm	-0.13	-0.02	0.05	0.04810	0.03680	76.69	20

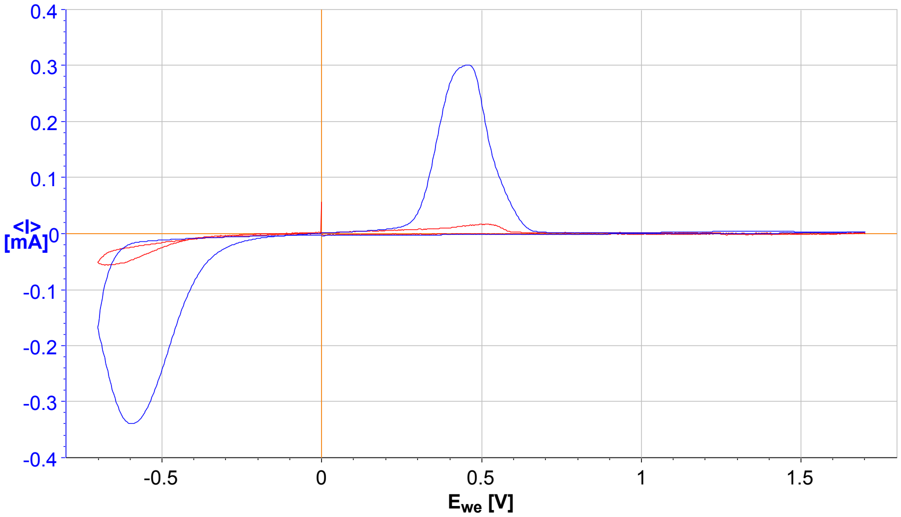

Figure 4.5: The first runs of the AT61 with 0.6 mm spacer (blue) and 0.8 mm spacer (red).

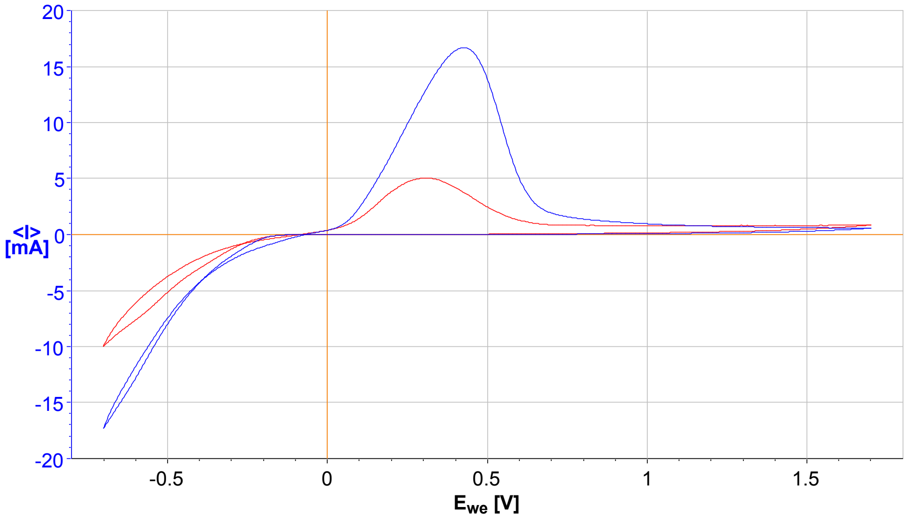

Figure 4.6: The last runs of the AT61 with 0.6 mm spacer (blue) and 0.8 mm spacer (red). For 0.6 mm, this is the 9th run and for 0.8 mm it is the 20th run.

4.2.4 Etching

AZ31 is the only alloy from which data obtained was obtained for both unetched (AZ31) and etched (AZ31e) electrodes. The data from these runs are presented in Table 4.4 and Table 4.5 and the first and and last runs of these specimens are shown in Figure 4.7 and Figure 4.8, respectively.

Table 4.4: The resistance and charge extracted from the CV for AZ31e and AZ31

Material	R_c [Ω]	R_a [Ω]	Q_c [mAh]	Q_a [mAh]	Eff [%]	Cycles
AZ31e$_{0.8}$	29.8	18.8	0.0826	0.0648	78.332	11*
AZ31$_{0.6}$	148.1	348.4	0.00803	0.00642	79.900000	21*

Table 4.5: The reversible potential, peak anodic potential and the overpotentials for AZ31 and AZ31e.

Material	E^{rev} [V]	$\eta_{c,1}$ [V]	$\eta_{a,1}$ [V]	$\eta_{c,end}$ [V]	$\eta_{a,end}$ [V]	Peak$_a$ [V]
AZ31e$_{0.8}$	-0.04	-0.53	0.30	-0.10	0.03	0.38
AZ31$_{0.6}$	-0.09	-0.54	0.44	-0.09	0.15	0.34

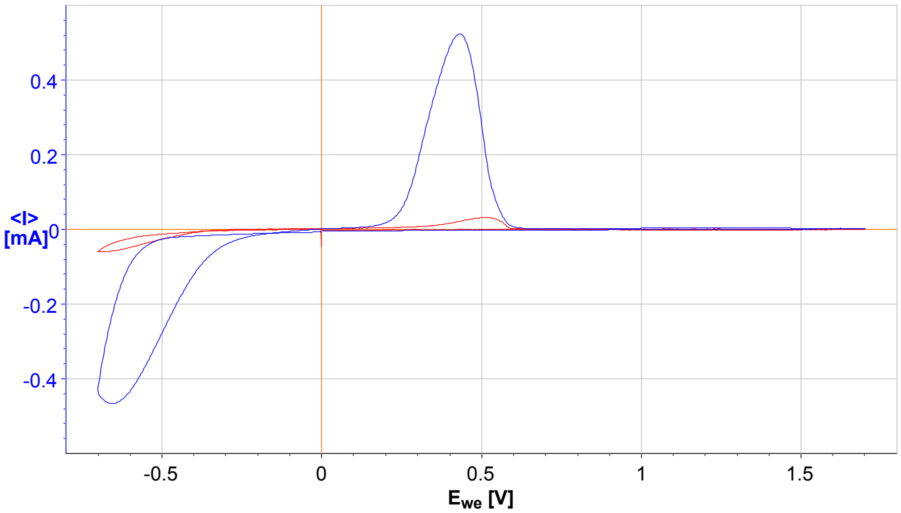

Figure 4.7: The first runs of the AZ31e$_{0.8}$ (blue) and AZ31$_{0.6}$ (red) electrodes.

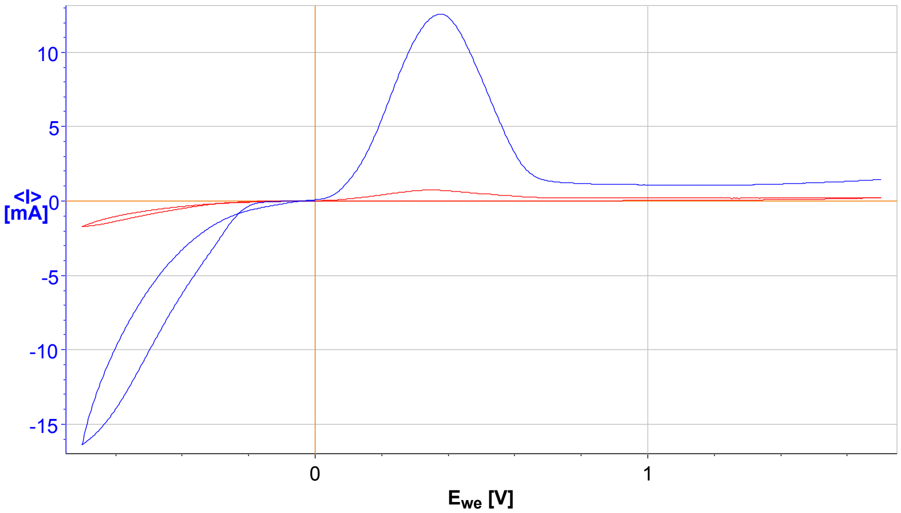

Figure 4.8: The last runs of the AZ31e$_{0.8}$ (blue) and AZ31$_{0.6}$ (red) electrodes. For AZ31e$_{0.6}$, this is the 11th run and for AZ31$_{0.6}$ it is the 21th run.

4.3 Cyclic Voltammetry

Because this is a project to demonstrate the feasibility of using cheaper Mg-alloys as electrode materials for magnesium batteries, the best results obtained for each alloy is chosen as the main results, whether that is the unetched or etched electrode. When investigating the cyclic voltammetry graphs, it is worth noting the difference in magnitude of the continuing current after the anodic peak.

4.3.1 Pure Magnesium

The full cyclic voltammogram of pure $Mg_{0.8}$ can be seen in Figure 4.9 and the data extracted from this are listed Table 4.6 in Table 4.7. The indicated coulombic efficiency was reached already in the second cycle.

Table 4.6: The resistance and charge extracted from the CV of $Mg_{0.8}$ cycled at 20 mV/s.

R_c [Ω]	R_a [Ω]	Q_c [mAh]	Q_a [mAh]	Eff [%]	Cycles
46.9	49.1	0.0640	0.0532	82.7	20

Table 4.7: The reversible potential, peak anodic potential and the overpotentials for $Mg_{0.8}$.

E^{rev} [V]	$\eta_{c,1}$ [V]	$\eta_{a,1}$ [V]	$\eta_{c,end}$ [V]	$\eta_{a,end}$ [V]	$Peak_a$ [V]
-0.02	-0.62	0.52	-0.20	0.03	0.40

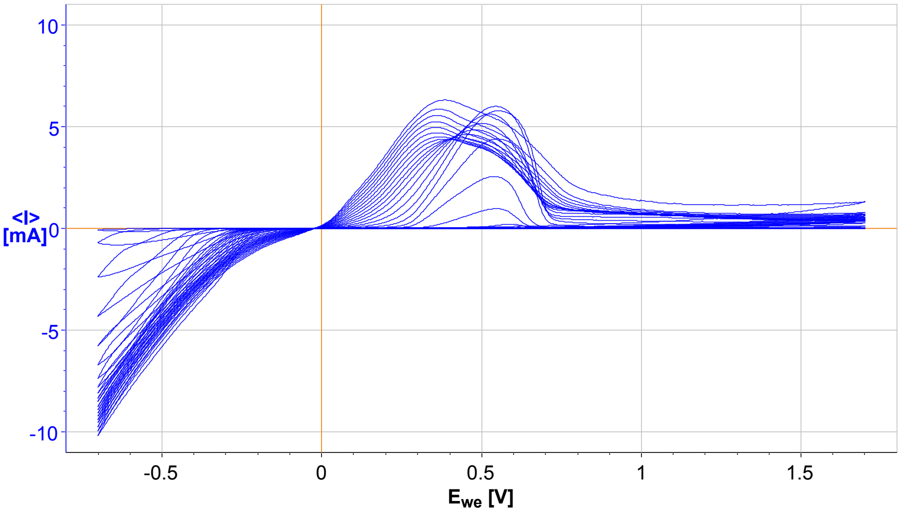

Figure 4.9: The full cyclic voltammogram of the 20 cycles before failure for $Mg_{0.8}$. The anodic peak shifts towards lower potentials with increasing cycle number.

4.3.2 AZ31

The full cyclic voltammogram of AZ31e$_{0.6}$ can be seen in Figure 4.10 and the data extracted from this are listed Table 4.8 and Table 4.9. These results were chosen over the results from AZ31 because of the lower resistance. The indicated coulombic efficiency was reached already in the second cycle.

Table 4.8: The resistance and charge extracted from the CV of AZ31e$_{0.6}$ cycled at 20 mV/s.

R$_c$ [Ω]	R$_a$ [Ω]	Q$_c$ [mAh]	Q$_a$ [mAh]	Eff [%]	Cycles
29.8	18.8	0.0826	0.0648	78.332	11*

Table 4.9: The reversible potential, peak anodic potential and the overpotentials for AZ31e$_{0.6}$.

E^{rev} [V]	$\eta_{c,1}$ [V]	$\eta_{a,1}$ [V]	$\eta_{c,end}$ [V]	$\eta_{a,end}$ [V]	Peak$_a$ [V]
-0.04	-0.53	0.3	-0.10	0.03	0.38

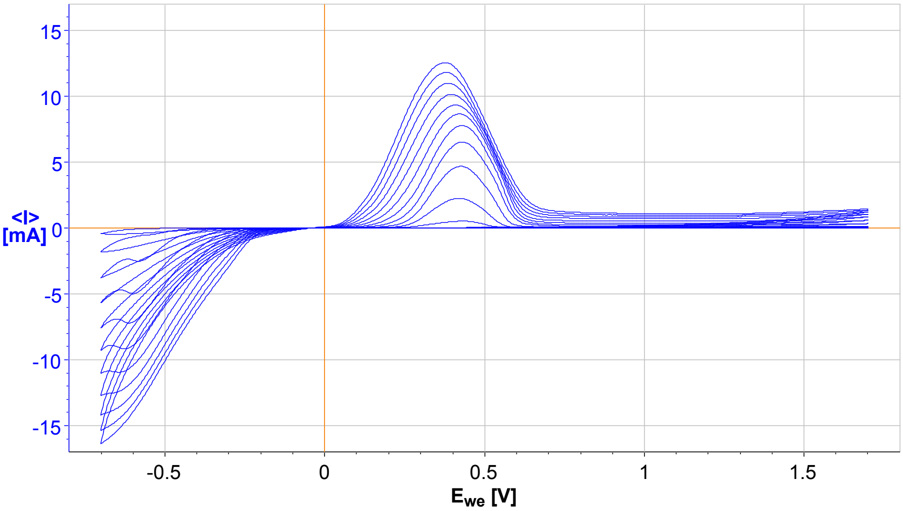

Figure 4.10: The full cyclic voltammogram of the 11 runs for AZ31e$_{0.6}$.

4.3.3 AZ61

The full cyclic voltammogram of AZ61e$_{0.6}$ can be seen in Figure 4.11 and the data extracted from this are listed Table 4.10$_{0.6}$ and Table 4.11. The coulombic efficiency approached 91% in the third cycle, 95% in the fifth cycle and were stable above 99% after the ninth cycle.

Table 4.10: The resistance and charge extracted from the CV of AZ61e$_{0.6}$ cycled at 20 mV/s.

R_c [Ω]	R_a [Ω]	Q_c [mAh]	Q_a [mAh]	Eff [%]	Cycles
19.8	19.6	0.140470	0.139426	99.2771	25

Table 4.11: The reversible potential, peak anodic potential and the overpotentials for AZ61e$_{0.6}$.

E^{rev} [V]	$\eta_{c,1}$ [V]	$\eta_{a,1}$ [V]	$\eta_{c,end}$ [V]	$\eta_{a,end}$ [V]	$Peak_a$ [V]
-0.06	-0.51	0.59	-0.10	0.04	0.43

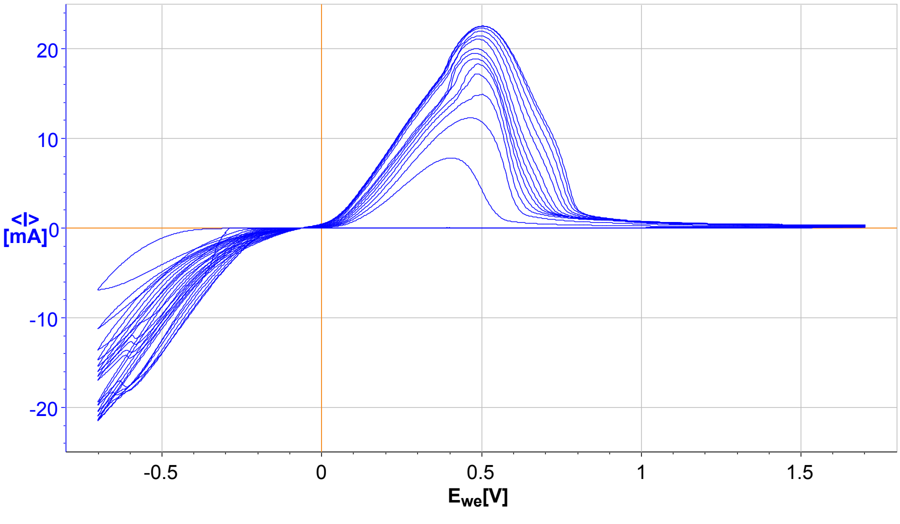

Figure 4.11: The full cyclic voltammogram of the last 14 cycles for AZ61e$_{0.6}$.

4.3.4 AT61

The full cyclic voltammogram for $AT61_{0.8}$ can be seen in Figure 4.12 and the data extracted are listed in Table 4.12 and Table 4.13. The indicated coulombic efficiency was reached in the fourth cycle.

Table 4.12: The resistance and charge extracted from the CV of $AT61_{0.8}$ cycled at 20 mV/s.

R_c [Ω]	R_a [Ω]	Q_c [mAh]	Q_a [mAh]	Eff [%]	Cycles
41.9	41.5	0.0481	0.0368	76.7	20

Table 4.13: The reversible potential, peak anodic potential and the overpotentials for $AT61_{0.8}$.

E^{rev} [V]	$\eta_{c,1}$ [V]	$\eta_{a,1}$ [V]	$\eta_{c,end}$ [V]	$\eta_{a,end}$ [V]	$Peak_a$ [V]
-0.13	-0.56	0.59	-0.02	0.05	0.31

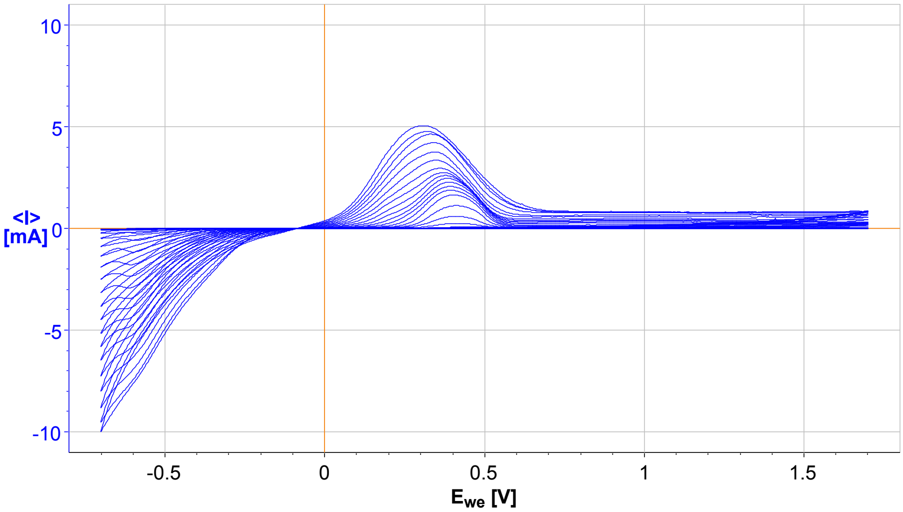

Figure 4.12: The full cyclic voltammogram for $AT61_{0.8}$ for the first 20 cycles.

4.3.5 AP65

The cyclic voltammogram of $AP65_{0.8}$ can be seen in Figure 4.13. This includes only the last 21 cycles and the data extracted from this are listed Table 4.14 and Table 4.15. The coulombic efficiency was continually rising from about 82% in the fourth cylce till it was stable above 99% in the 12th cycle.

Table 4.14: The resistance and charge extracted from the CV of $AP65_{0.8}$ cycled at 20 mV/s.

R_c [Ω]	R_a [Ω]	Q_c [mAh]	Q_a [mAh]	Eff [%]	Cycles
106.3	138.2	0.0335	0.0332	99.2	32*

Table 4.15: The reversible potential, peak anodic potential and the overpotentials for $AP65_{0.8}$.

E^{rev} [V]	$\eta_{c,1}$ [V]	$\eta_{a,1}$ [V]	$\eta_{c,end}$ [V]	$\eta_{a,end}$ [V]	$Peak_a$ [V]
-0.11	-0.52	0.47	-0.06	0.02	0.54

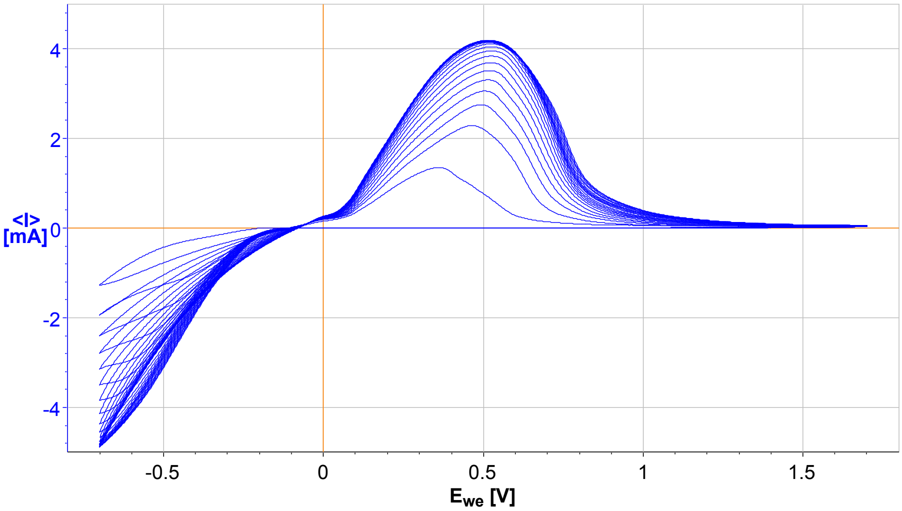

Figure 4.13: The last 21 cycles of the cyclic voltammogram of $AP65_{0.8}$.

4.3.6 Untreated Alloys

As mentioned, a series of runs were done without any prior surface treatment of the electrodes. The results of these runs are shown in Figure 4.14. It can easily be seen that the only alloy showing reversible potential is AP65u and the data for this alloy are presented in Table 4.16

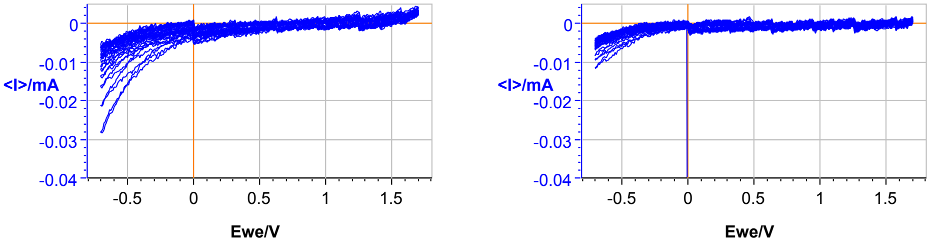

(a) AZ31$u_{0.8}$ (b) AZ61$u_{0.8}$

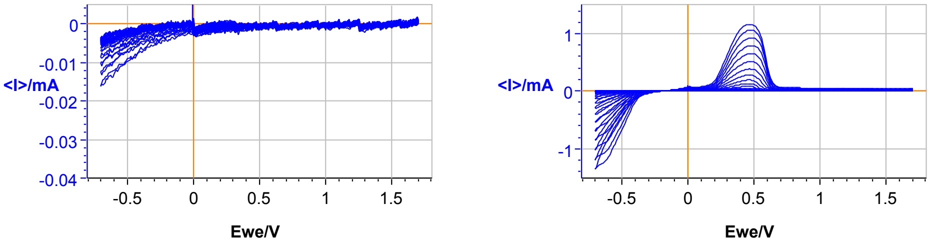

(c) AT61$u_{0.8}$ (d) AP65$u_{0.8}$

Figure 4.14: Cyclic voltammograms of the four untreated alloys. Notice the difference in the scale between the AP65$u_{0.8}$ graph and the other graphs.

Table 4.16: The results of the CV of AP65$u_{0.8}$ cycled at 20 mV/s

E^{rev} [V]	η_c [V]	η_a [V]	Q_c [mAh]	Q_a [mAh]	Eff [%]	Cycles
-0.15	-0.22	0.3	0.00499	0.00439	88.59	21*

4.3.7 Intercalation Electrodes

The cyclic voltammogram of Mg, AZ61 and AZ61e vs. V_2O_5 can be seen in Figure 4.15. This is the second cycle of the CV at 1 mV/s. The CV recorded at 10 µV/s did not yield any results.

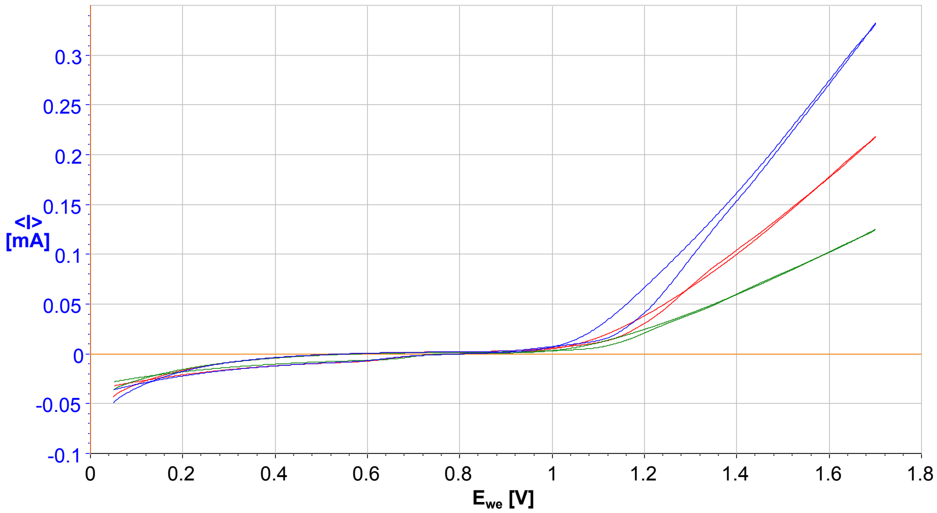

Figure 4.15: The second cycle of the CV's of Mg (green), AZ61e (red) and AZ61 (blue) vs. V_2O_5, cycled at 1 mV/s.

4.4 Electrolyte Stability

The best data for assessing the electrolyte stability was actually recorded with the untreated alloys, as these cells did not experience a failure during cycling. The LSV-data for these alloys are shown in Figure 4.16.

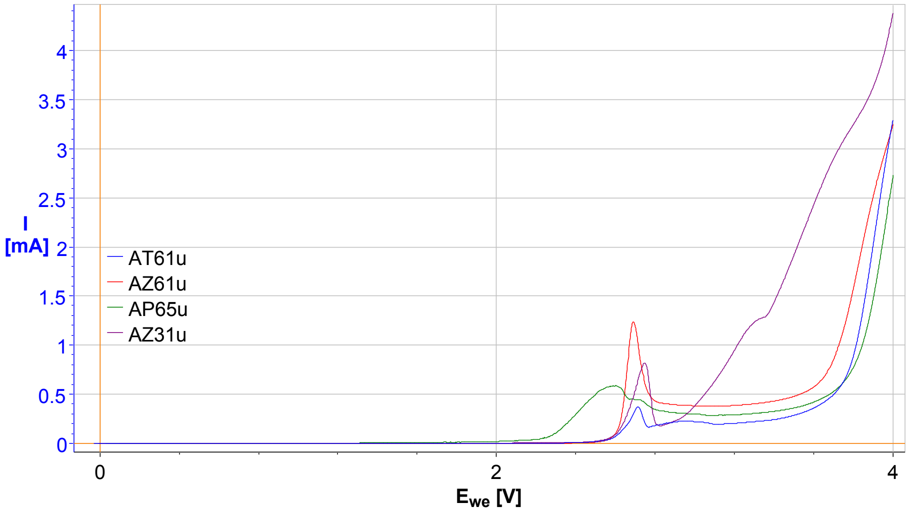

Figure 4.16: The LSV-sweep on the untreated alloys. Sweep rate 20 mV/s.

4.5 SEM and EDS

EDS-spectra was recorded for all the areas shown in the following micrographs. These are included in Appendix B and the assessment of these are given in each section. In the EDS-spectras for the Cu-electrodes the general trend is that areas with high signal from copper have no signal from magnesium and vice versa. Another trend is that areas on the Mg-electrodes that looks like re-deposited Mg often have a higher signal from Cl, Al and C.

Unfourtunatly, SEM and EDS data were only acquired for the materials listed here, due to the other electrodes not being kept for SEM-analysis.

4.5.1 Mg

SEM-pictures of the the two electrodes used in the Mg-cell are shown in Figure 4.17. From the EDS-spectra it was found dark areas on the Cu are deposited Mg and the dark structures on the Mg-electrode have low Mg-signal and increased signal from Cl, Al and C.

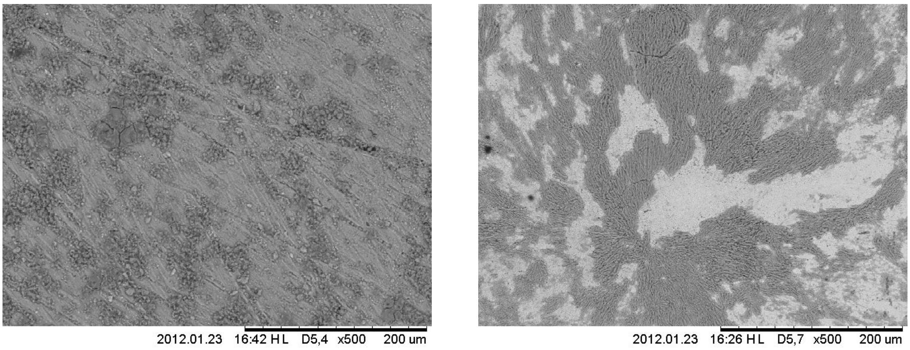
2012.01.23 16:42 H L D5,4 x500 200 um
2012.01.23 16:26 H L D5,7 x500 200 um

(a) Mg

(b) Cu

Figure 4.17: The two electrodes of an Mg-cell after cycling. Recorded at 15 kV.

4.5.2 AZ31

SEM-pictures of the the two electrodes used in the AZ31e-cell are shown in Figure 4.18. From the EDS-spectra it was found that the flakes on the Cu are deposited Mg and the darker areas on the AZ31e-electrode have low Mg-signal and increased signal from Cl, Al and C. No signal from zinc was recorded on the Cu-electrode.

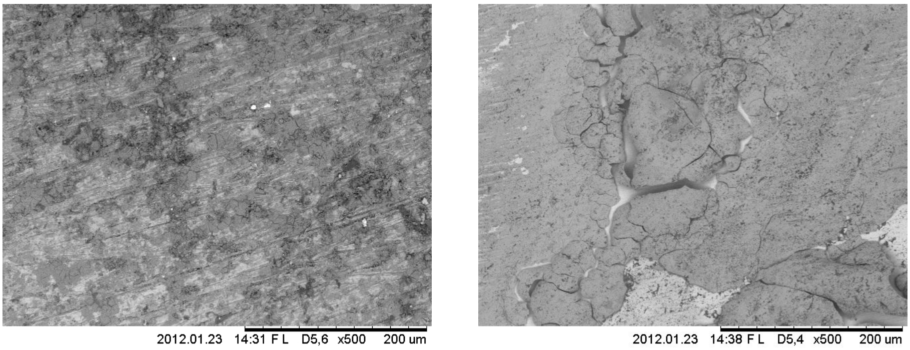
2012.01.23 14:31 F L D5,6 x500 200 um
2012.01.23 14:38 F L D5,4 x500 200 um

(a) AZ31e

(b) Cu

Figure 4.18: The two electrodes of an AZ31e-cell after cycling. Recorded at 5 kV.

4.5.3 AP65

SEM-pictures of the the two electrodes used in the AP65-cell are shown in Figure 4.19. From the EDS-spectra it was found dark areas on the Cu are deposited Mg and the broken-up structures on the AZ31e-electrode have low Mg-signal and increased signal from Cl, Al and C. No signal from lead was recorded on the Cu-electrode.

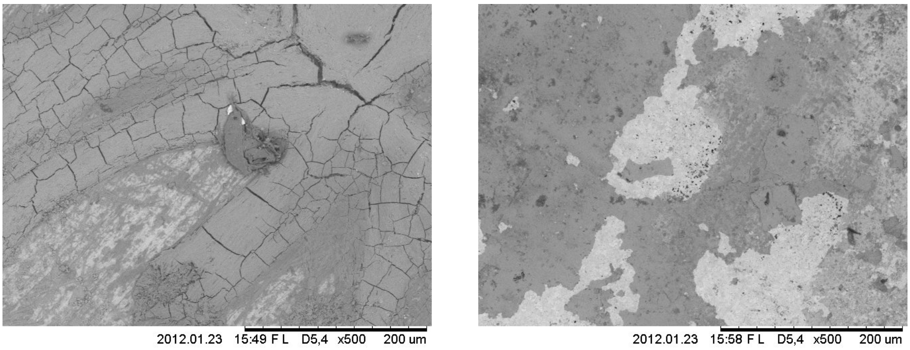
2012.01.23 15:49 F L D5,4 x500 200 um
2012.01.23 15:58 F L D5,4 x500 200 um

(a) AP65

(b) Cu

Figure 4.19: The two electrodes of an AP65-cell after cycling. Recorded at 5 kV.

4.6 Practical

After opening the container with the pure magnesium sheet it quickly became covered in a white layer. This seemed to grow when exposed to air and it became increasingly harder to remove using chromium acid. After the etching the metal was relatively shiny, but a white layer managed to grow on it when exposed to air during the transfer from the acid-bath to the glovebox (about 10 minutes).

All the alloys were shiny metal sheets when they arrived and storing in air did not have any noticeable effects.

The price of the 10×10 cm 99.9% pure magnesium sheet was €381. All the alloys were bought in sheets of 20×20 cm for €16.

5 Discussion

5.1 External Reference

The data presented in section 4.2.2 show a stable reversible potential of approx -0.25 V, for both electrodes which would suggest that the electrode potential of the given material is 0.25 V below the electrode potential of Mg^{+}/Mg. This is however very unlikely as the reactions happening at the working electrode should be exactly the same as the reactions happening at the reference electrode in the case of Mg-anode.

The reason why the reversible potential is different from 0 V is not completely understood, but it is probably a combination of different levels of oxidation of the electrodes and increased electrolyte resistance between the WE and REF.

Due to the fact that they have a reversible potential close to -0.25 V, they were cycled to -0.45 V and to 1.95 V compared to the reversible potential. This means that a lot less material were plated from the Mg-electrodes to the copper foil, and that the anodic voltage approached the breakdown voltage of the electrolyte, decreasing the number of cycles they could sustain. Therefore, the results from the 3-electrode cell are not used for calculations concerning the viability of different electrode materials.

5.2 Kinetics

The kinetics of the electrodes are fast enough for cycling at 20mV/s. This can be seen from Figure 4.3 by the fact that there is a negible change in the shape of the CV with decreasing scan speed. If the kinetics were the determining factor of the shape of the CV, the computed resistance would increase with increasing scan speeds.

What we do see at the decreased speed, is that the battery could only sustain 3 complete cycles before experiencing a total failure. This is probably due to the effect of more material being plated back and forth, and this effect is discussed in greater detail in section 5.5.

It is however only the internal resistance and overpotentials of the given materials that is determining the shape of the cyclic voltammogram, meaning that cyclic voltammetry at 20mV/s is an appropriate tool for investigating the characteristics of the given electrode material.

5.3 Internal Pressure

It is clear from the data presented in section 4.2.3 that the resistance is increased with increasing internal pressure. The cells with higher internal pressure were also able to sustain significantly higher number of charge-cycles, but this is probably an effect due to less material being plated back and forth and again, this effect is discussed in section 5.5.

5.4 Etching

It is clear from the results from the untreated alloys, presented in section 4.3.6, that some surface treatment is required before using the alloys in a battery. AP65, which is especially engineered by *Magnesium Elektron* to be used in primary backup-batteries, shows reversible plating and re-deposition. However, it is clear from comparing the AP65u graph with the AP65 graph that the latter has improved characteristics.

The results presented for AZ31 and AZ31e in section 4.2.4 also clearly suggest that the etched samples are better in most respects than the not-etched samples. There is however another very important difference between the two samples, and that is the internal pressure discussed in the previous section. Therefore, these results are not good enough to differentiate whether etching is essential for the performance of the electrodes.

Good results have also been acquired with unetched samples, such as AP65 and AT61 suggesting that thorough abrasion of the surface prior to assembly is a satisfactory treatment for the alloys.

It is therefore difficult to say anything conclusive whether etching is necessary as a surface treatment, but it shows that with correct surface treatment, alloys stored in air can be used in batteries, as opposed to pure lithium or magnesium.

5.5 Charge Capacity and Efficiency

The results obtained for Mg, AZ31 and AT61 are similar in many respects. The resistance for all three are of similar size and the coulombic efficiency is between 76% and 83%, which is what we would expect with the given electrolyte. These electrodes also exhibit a continuing anodic current after the re-deposition peak, suggesting that the re-deposition is not complete and that it continues throughout the cycle.

The two electrode materials that distinguishing themselves are the AZ61 and the AP65. Both exhibit over 99% efficiency which is way over what should be expected with the given electrolyte. However, the resistance of the two differs significantly, and as a result the amount of material plated back and forth is almost 40 times higher for the AZ61. Both these alloys show a current close to zero in the area after the anodic peak, which further underlines that that the re-deposition is almost complete.

Both these alloys were also the ones being able to sustain the highest amount of cycles before experiencing a failure. AZ61 was cycled 25 times before submitting and AP65 was cycled over 30 times before the CV's were stopped.

AZ61 is also the alloy with the highest absolute charge being cycled. But, using the data from section 4.3.3 and the average density of magnesium we find out that this corresponds to an average thickness of the plated layer of only about 0.24 µm. The data suggest that cycling any deeper than that will quickly bring an end to the batteries, decreasing the usefulness of these metal electrodes.

This very important correlation, mentioned before, is the correlation between the amount of material cycled per cycle and the number of cycles a battery could sustain. For the AT61-electrodes presented in section 4.2.3 it is clear that the decreased internal pressure reduced the resistance and allowed more material to be plated and re-deposited. These batteries failed at a much lower cycle number suggesting that a coin cell of this construction, with electrodes of Mg and Cu-foil, can only transfer a limited amount of material between the electrodes before failing.

However, the fact that coin-cells with close to 100% cycling efficiency can sustain a larger number of cycles, at even higher charge rates for the AZ61, suggest that the problem might be on the copper foil where Mg will build up in subsequent cycles. This is partly confirmed with the SEM-analysis, see section 5.7

5.6 Resistance and Overpotentials

The resistance, as the charge capacity, is greatly dependent on the internal pressure and possibly pre-treatment, and it is difficult to separate these factors based on the given limited data set. It seems however that the overpotentials at which the activation energy barrier is overcome are relatively independent of the environmental conditions and are an intrinsic material property.

After the initial cycling the cathiodic overpotential stabilized at around -0.2 V for Mg, -0.1 V for most of the alloys and only -0.02 V for AT61. Using Equation 2.1 we see that this correspond to an activation energy of 38.6 kJ/mol, 19.3 kJ/mol and 3.9 kJ/mol, respectively. The anodic overpotentials are all very similar corresponding to an activation energy of approx 5.8 kJ/mol

5.7 Deposit Structure and Composition

From the SEM-images it is clear that the metal deposited on the copper from the pure Mg has a much finer structure, with fine, needle-like structures rising from the surface. It is also clear that the deposited metal on Cu from the Al-containing electrodes has a much smoother surface. It seems however, that some of these deposits are not very well attached to the surface, especially for AZ31e. If these deposits flake off, it could contribute to irreversible capacity losses.

The EDS-spectra show a relatively even distribution of C over the sample, indicating a pretty even layer of dried-up electrolyte on the surface. The signals also show that O-response comes from the same areas as Mg, indicating that most of the Mg is oxidized, probably when transferred in air from the glove box to the lab for SEM-study. Most of the deposits also show a high signal from Cl, indicating that some electrolyte might be incorporated in the deposits. If this is the case, it could be seriously deteriorating for the battery.

The EDS-spectra also shows that none of the alloying elements is transferred back and forth, with the possible exception of Al, which gives a high response on the Cu-electrodes. It is though, also a major constituent of the electrolyte and it is difficult to determine whether the signal comes from dried-up electrolyte or deposited metal. One factor in favor for the latter is that for the two cells investigated with Al-containing alloys, the Al-signal comes mainly from the same areas as the Mg-signal. This is not the case for the Cu-electrode from the pure Mg cell, where all the Al must come from the electrolyte.

5.8 Effect of Alloying Elements

The results so far seems to indicate that high levels of aluminum (6 wt%) increases the usability of magnesium alloys. These alloys exhibit much smoother deposits on the Cu-foil and show much higher coloumbic efficiency. The reason for this could be a positive interaction between the aluminum in the electrolyte and the transferred aluminium.

The lead-containing alloy (AP65) does exhibit the same positive effects, but displays higher resistance. It is impossible to say whether this is because of an inherent material property or due to the increased internal pressure of that particular cell.

AT61 is the only alloy with high Al-content that does not seem to exhibit these positive properties. There might be several reasons for that, and one explanation might be that the less negative reduction potential of Tin (-0.12 V) is inhibiting the transfer of Mg and possibly Al.

5.9 Intercalation Electrodes

The data from the cells assembled with intercalation electrodes show that all the three tested electrodes, Mg, AZ61 and AZ61e, exhibit a reversible potential against the V_2O_5 of about 0.8 V. This is in accordance with literature. The graphs, however, indicate that much more magnesium is de-intercalated, than is intercalated. This means that some secondary reactions are taking place giving us the increased current response. These reactions might include electrolyte decomposition, electrode material degeneration or vanadium being plated on the Mg-electrode.

Therefore, no conclusion can be given with the respect of using these alloys against an proper cathode, but they do indicate that the behavior of Mg, AZ61 and AZ61e are similar.

5.10 Electrolyte Stability

The results confirms the findings of Aurbach et al.[29] that versus magnesium, the $(BuAlCl_3)_2Mg$, has an efficiency of around 80% and a an aniodic breakdown voltage of 2.2 V. The results indiate however that the efficiency is greatly increased when cycled against less reactive magnesium alloys, suggesting that the real trouble lies with using highly active magnesium.

It is also worth noting that assessing the electrolyte stability using the alloy that had already been cycled, AP65u, the on-set of the anodic peak indicating electrolyte decomposition happens at lower potential. This shows that cycling the coin-cells alters the electrochemical stability of the electrolyte, meaning that the breakdown of the other cells might be caused by electrolyte decomposition as a function of this. Further work with other electrolytes will determine if this is the case.

5.11 Practical

The price for producing an alloy or metal will of course be influenced be several factors, such as availability and demand, but the ultimate cost is determined by the ease of making a given material from raw materials. The prices paid for the different electrode materials for this thesis therefore serves as a good indicator of the price difference and it shows that pure Mg is roughly 100 times more expensive than the alloys.

6 Conclusion

In this thesis, data have been obtained to show that magnesium alloys offer a good or better alternative to pure magnesium in magnesium ion-transfer batteries. They are significantly cheaper, by a factor 100, and are largely unaffected by long-time storage in air. The performance of all alloys is dependent on the surface treatment prior to assembly, and for alloys, etching in chromium acid and/or polishing are appropriate treatments.

Aluminum content of about 6% seems to improve the charge-discharge characteristics and by enhancing the structure of the cycled materials. With respect to which alloy is the better, the data is not complete enough to conclusively single out one alloys that is superior to the other. In this study however, AZ61 is the top performer with a coulombic efficiency of close to 100%, the lowest resistance in the coin-cells and the alloy being able to sustain the highest amount of charging. Although showing the highest resistance of the tested alloys, AP65 is the only other alloy reaching this coulombic efficiency and the only alloy showing reversible dissolution and re-deposition untreated.

It seems however that batteries based on metal anodes, still are a long way from being top performers among secondary batteries, since even the top performers can sustain relatively few charge cycles at low charge densities before deteriorating beyond usability. Metal anodes might however be good enough for initial magnesium-ion batteries.

7 Further Work

7.1 Extending This Thesis

In order to obtain conclusive evidence which is the better alloy for these purposes, more tests are needed. This should be a larger-scale experiments with multiple cells made with each alloy. SEM and EDS-studies should be carried out on all these electrodes. Three-electrode cells should also be used to conclusively determine the reduction potentials of the alloys versus Mg^+/Mg.

A second series of experiments should also be carried out with an improved electrolyte, such as the 'All phenyl complex' to see if more cycles can be sustained with this electrolyte. In addition, another and improved cast of V_2O_5 should also be made and the properties of the alloys when cycled against a working intercalation anode should be assessed.

7.2 Magnesium-ion Batteries

After two decades of research it seems like the field of magnesium-ion batteries have matured quite a lot in terms of electrolytes and anode materials. The biggest challenge still faced in the field are the lack of suitable cathode materials with a descent voltage against Mg^+/Mg and satisfactory charge density. If a cathode material were to be found, secondary magnesium-ion batteries would be good enough to compete commercial batteries, at least in some categories such as price. As commercial interest increases, development tends to accelerate and the technology would probably mature towards a level where it can compete in most categories with lithium-ion batteries.

Until such a suitable cathode material is found, secondary magnesium-ion batteries seems unlikely.

Bibliography

[1] Andreas Dinger, Ripley Martin, Xavier Mosquet, Maximilian Rabl, Dimitrios Rizoulis nad Massimo Russo, and Georg Sticher. Batteries for electric cars. Technical report, The Boston Consulting Group, 2010.

[2] William Tahil. The trouble with lithium. Technical report, Meridian International Research, 2005.

[3] R. Holze. Table 1.1. metal electrode potentials in aqueous electrolyte systems. In *Landolt-Börnstein - Group IV Physical Chemistry*, volume 9A. Springer-Verlag, 2007.

[4] R. D. Shannon. Revised effective ionic radii and systematic studies of interatomic distances in halides and chalcogenides. *Acta Crystallographica Section A*, 32(5):751–767, Sep 1976.

[5] I. Jackson. 2.4.3 the crust. In *Landolt-Börnstein - Group V Geophysics*, volume 2a.

[6] C.H. Hamann, A. Hamnett, and W. Vielstich. *Electrochemistry.* Wiley-VCH, second, completely updated and revised edition edition, 2007.

[7] Asmund Sterten. *Lecture notes TMT4252, electrochemistry.* NTNU, 1995.

[8] Jr. David K. Gosser. *Cyclic Voltammetry: simulation and analysis of reaction mechanisms.* VCH Publishers, Inc., 1993.

[9] F. Orsini, A. Du Pasquier, B. Beaudoin, J. M. Tarascon, M. Trentin, N. Langenhuizen, E. De Beer, and P. Notten. In situ scanning electron microscopy (sem) observation of interfaces within plastic lithium batteries. *Journal of Power Sources*, 76(1):19 – 29, 1998.

[10] Mee Kyung Song, Seung Do Hong, and Kyoung Tai No. The structure of lithium intercalated graphite using an effective atomic charge of lithium. *Journal of The Electrochemical Society*, 148(10):A1159–A1163, 2001.

[11] M Broussely, S Herreyre, P Biensan, P Kasztejna, K Nechev, and R.J Staniewicz. Aging mechanism in li ion cells and calendar life predictions. *Journal of Power Sources*, 97-98:13 – 21, 2001. Proceedings of the 10th International Meeting on Lithium Batteries.

[12] Kang Xu. Nonaqueous liquid electrolytes for lithium-based rechargeable batteries. *Chemical Reviews*, 104(10):4303–4418, 2004.

[13] Perla B. Balbuena and Yixuan Wang, editors. *Lithium-Ion Batteries : Solid-Electrolyte Interphase.* Number 9781860946448. Imperial College Press, London, GBR, 2003.

[14] Pallavi Verma, Pascal Maire, and Petr Novak. A review of the features and analyses of the solid electrolyte interphase in li-ion batteries. *Electrochimica Acta*, 55(22):6332 – 6341, 2010.

[15] Masaki Yoshio, Ralph J. Brodd, and Akiya Kozawa, editors. *Lithium-Ion Batteries Science and Technologies*. Springer Science+Business Media, 2009.

[16] J. C. Slater. Atomic radii in crystals. 41(10):3199–3204, 1964.

[17] I. Jackson. 2.4.4 the upper mantle. In *Landolt-Börnstein - Group V Geophysics*, volume 2a.

[18] D.R. Askeland and P. Webster. *The science and engineering of materials*. Chapman and Hall, 1990.

[19] W.D. Callister and D.G. Rethwisch. *Materials Science and Engineering*. Wiley, 2010.

[20] E. Levi, Y Gofer, and D. Aurbach. On the way to rechargeable mg batteries: The challenge of new cathode materials. *Chemistry of Materials*, 22(3):860–868, 2010.

[21] Petr Novàk, Valery Shklover, and Reinhard Nesper. Magnesium insertion in vanadium oxides: A structural study. *Zeitschrift für Physikalische Chemie*, 185(Part 1):51–68, January 1994.

[22] Petr Novàk, Werner Scheifele, Felix Joho, and Otto Haas. Electrochemical insertion of magnesium into hydrated vanadium bronzes. *Journal of The Electrochemical Society*, 142(8):2544–2550, 1995.

[23] Daichi Imamura and Masaru Miyayama. Characterization of magnesium-intercalated v2o5/carbon composites. *Solid State Ionics*, 161(1-2):173 – 180, 2003.

[24] Lifang Jiao, Huatang Yuan, Yijing Wang, Jiansheng Cao, and Yongmei Wang. Mg intercalation properties into open-ended vanadium oxide nanotubes. *Electrochemistry Communications*, 7(4):431 – 436, 2005.

[25] Roger Chevrel, Marcel Sergent, and Jacques Prigent. Un nouveau sulfure de molybdene : Mo3s4 preparation, proprietes et structure cristalline. *Materials Research Bulletin*, 9(11):1487 – 1498, 1974.

[26] D. Aurbach, Z. Lu, A. Schechter, Y. Gofer, H. Gizbar, R. Turgeman, Y. Cohen, M. Moshkovich, and E. Levi. Prototype systems for rechargeable magnesium batteries. *Nature*, 407(6805):724–727, October 2000.

[27] C. LIEBENOW. Reversibility of electrochemical magnesium deposition from grignard solutions. *Journal of Applied Electrochemistry*, 27:221–225, 1997. 10.1023/A:1018464210084.

[28] J.A. Dean. Lange's handbook of chemistry (15th edition), 1999.

[29] Doron Aurbach, Haim Gizbar, Alex Schechter, Orit Chusid, Hugo E. Gottlieb, Yossi Gofer, and Israel Goldberg. Electrolyte solutions for rechargeable magnesium batteries based on organomagnesium chloroaluminate complexes. *Journal of The Electrochemical Society*, 149(2):A115–A121, 2002.

[30] Pred materials international. http://www.predmaterials.com/hohsen/HS3ETestCell.html, 12 2011.

A Materials and chemicals

Table A.1 list the full specifications of the chemicals used in this thesis.

Table A.2 list the full specifications of the alloys used in this thesis. The alloys and the specifications are obtained from *Magnesium Elektron*. Blank spaces indicates where no data was provided from the producer and the symbol ‘<’ is used to indicate values below the detection limit.

Table A.1: Materials and chemical used during this project

Material	Formula	Producer	Purity	Usage	Remarks
PVDF	$-(C2H2F2)n-$	Kynar RC	Fine Powder	Binder	poly-1,1-difluoroethene
NMP	C_5H_9NO	Sigma-Aldrich	$> 99.0\%$	Solvent	1-Methyl-2-pyrrolidone
EC	$C_3H_4O_3$	Sigma Aldrich	$> 99\%$	Electrolyte solvent	Ethylene carbonate
DEC	$C_5H_{10}O_3$	Sigma	$> 99\%$	Electrolyte solvent	Diethyl carbonate
$LiPF_6$	$LiPF_6$	Aldrich	99.99%	Electrolyte salt	Lithium hexaflourophosphate
Lithium	Li	Alfa Aeser	99.90%	Anode	Lithium foil
Copper	Cu		n/a	Cathode substrate	Copper sheets
V_2O_5	V_2O_5	Sigma-Aldrich	98%	Cathode material	Vanadium(V) oxide

Table A.2: Full specifications of the magnesium alloys used in this thesis. The magnesium is acquired from Alfa Aesar and the alloys from from Magnesium Elektron.

Material	Al wt%	Ca wt%	Cu wt%	Fe wt%	Mn wt%	Ni wt%	Pb wt%	Si wt%	Sn wt%	Zn wt%	Zr	TO
Magnesium												<0.001
AZ31	3.0	<0.01	<0.001	0.002	0.19	0.0006		0.02		0.71	<0.01	<0.3
AZ61	6.2	<0.01	<0.001	0.001	0.22	0.0009	<0.01	0.02		0.61	<0.01	<0.30
AT61	6.0	<0.01	<0.001	0.002	0.01	0.0004		0.02	1.0	<0.01		<0.30
AP65	6.3	<0.01	0.002	0.001	0.18	<0.001	4.7	<0.01		0.6		<0.3

TO = Total Others

B EDS spectra

In the following section, EDS-data are prestented. The big, unmarked peaks in the EDS-spectras of the Cu-electrodes are secondary Cu-lines.

B.1 Mg

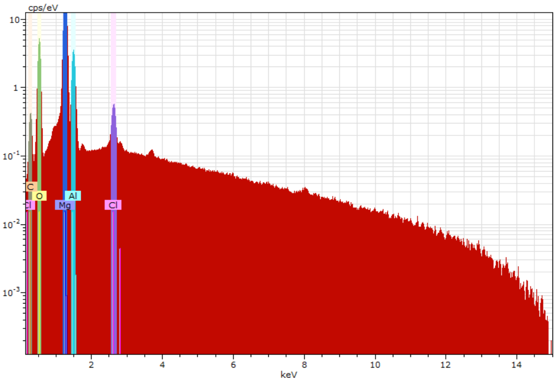

(a) EDS-spectra

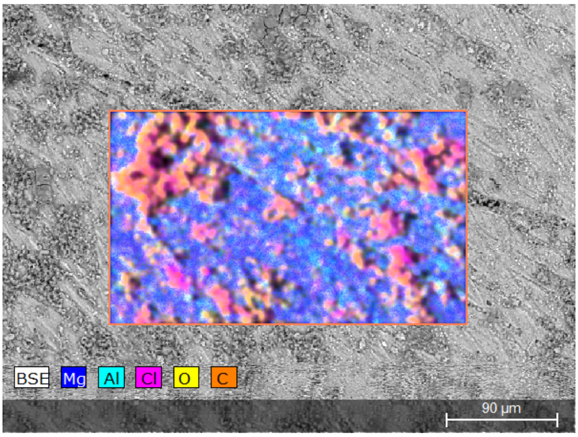

(b) EDS-map

Figure B.1: EDS data from the Mg-electrode in the $\mathrm{Mg}_{0.8}$-cell.

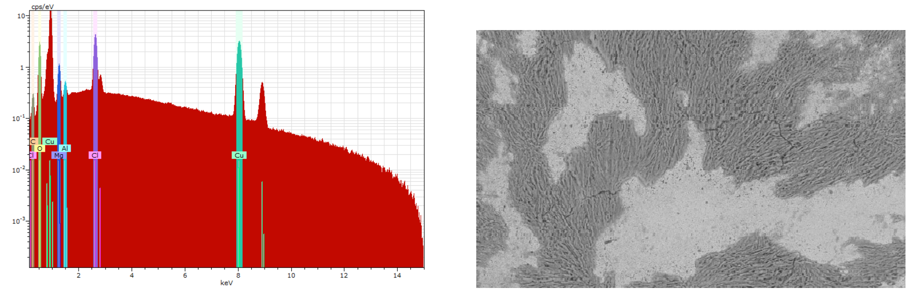

(a) EDS-spectra

(b) BSE-image

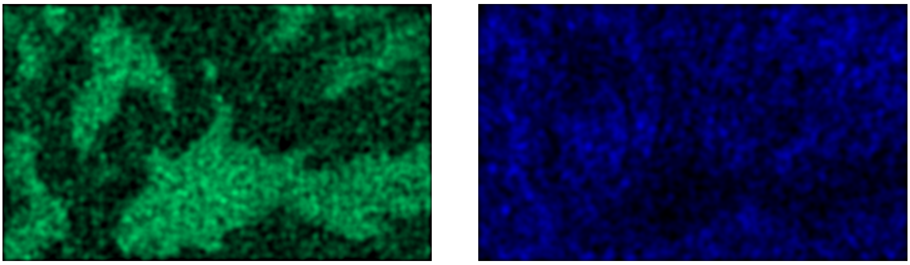

(c) Cu-map ($K\alpha$-line)

(d) Mg-map (K-line)

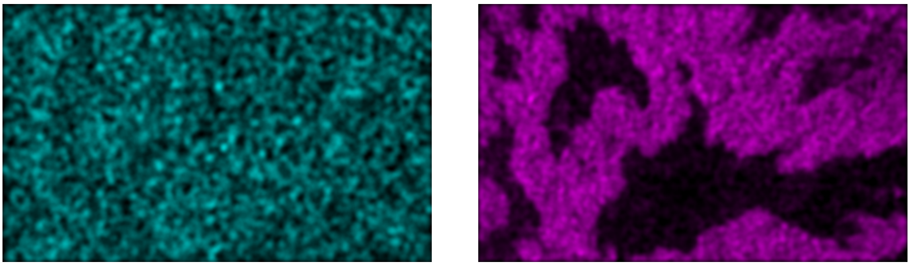

(e) Al-map (K-line)

(f) Cl-map ($K\alpha$-line)

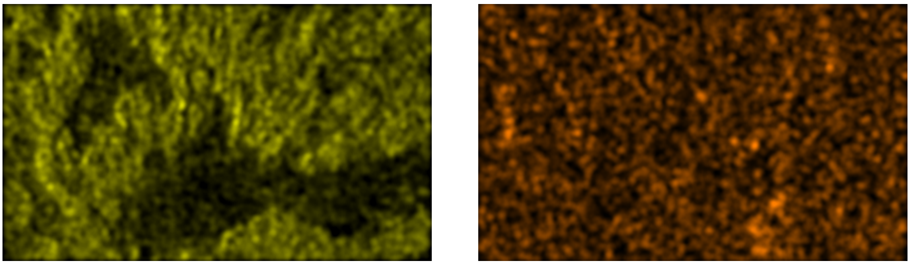

(g) O-map ($K\alpha$-line)

(h) C-map ($K\alpha$-line)

Figure B.2: EDS data from the Cu-electrode in the $Mg_{0.8}$-cell.

B.2 AZ31e

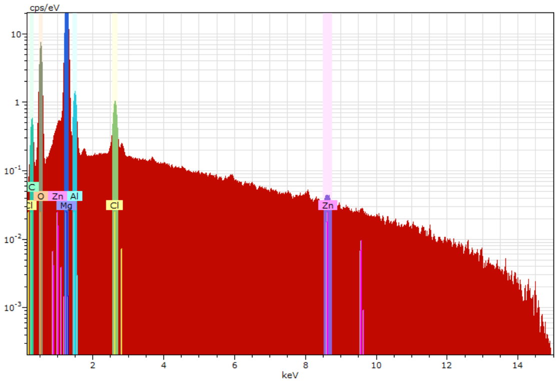

(a) EDS-spectra

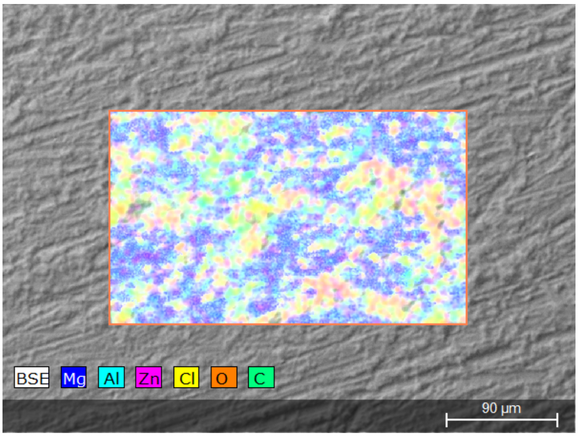
BSE
Mg
Al
Zn
Cl
O
C
90 µm

(b) EDS-map

Figure B.3: EDS data from the AZ31e-electrode in the AZ31e$_{0.6}$-cell.

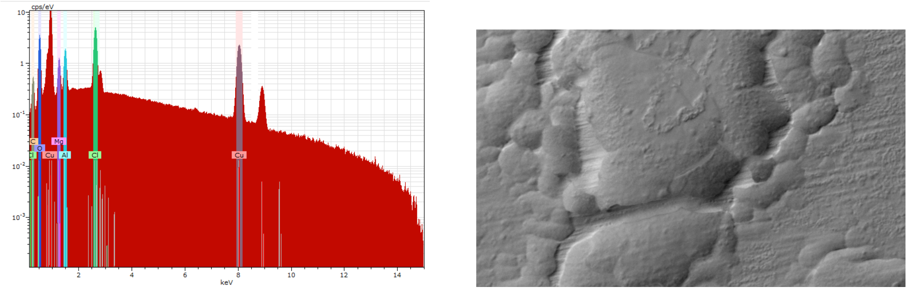

(a) EDS-spectra (b) BSE-image

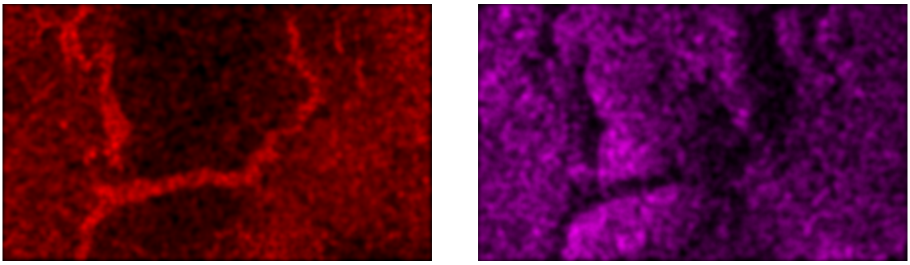

(c) Cu-map ($K\alpha$-line) (d) Mg-map (K-line)

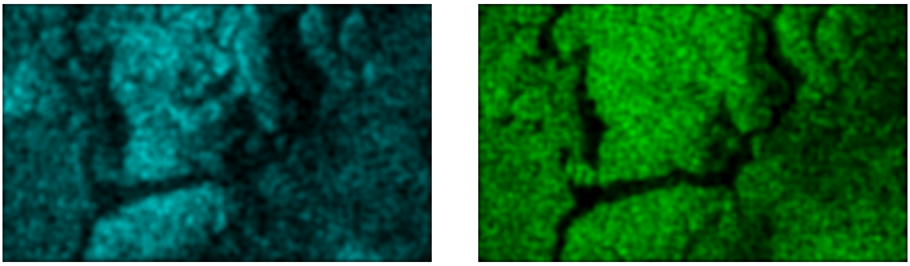

(e) Al-map (K-line) (f) Cl-map ($K\alpha$-line)

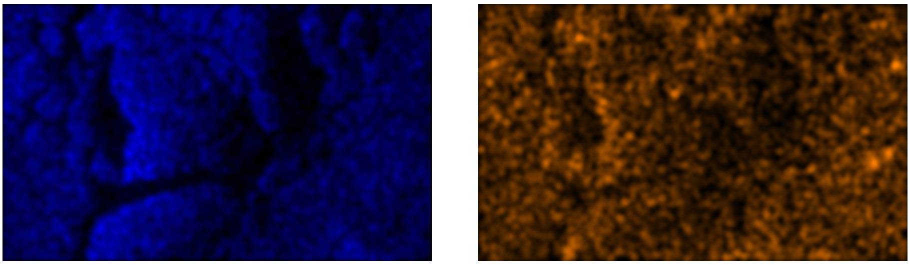

(g) O-map (K-line) (h) C-map ($K\alpha$-line)

Figure B.4: EDS data from the Cu-electrode in the AZ31e$_{0.6}$-cell.

B.3 AP65

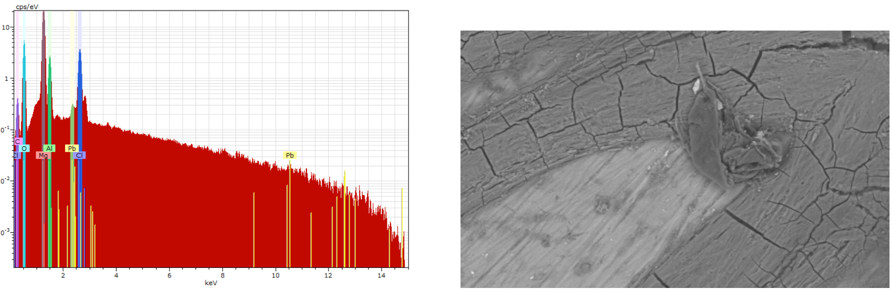

(a) EDS-spectra (b) BSE-image

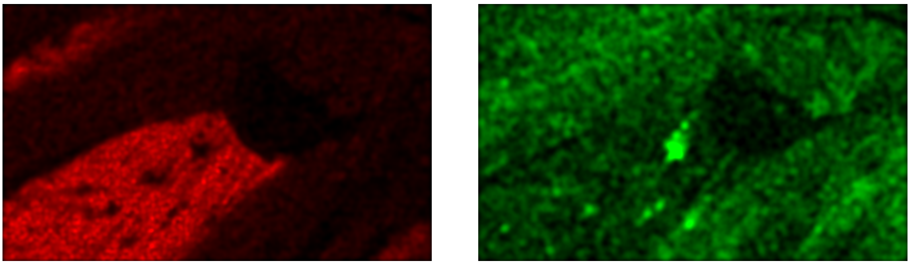

(c) Mg-map (K-line) (d) Al-map (K-line)

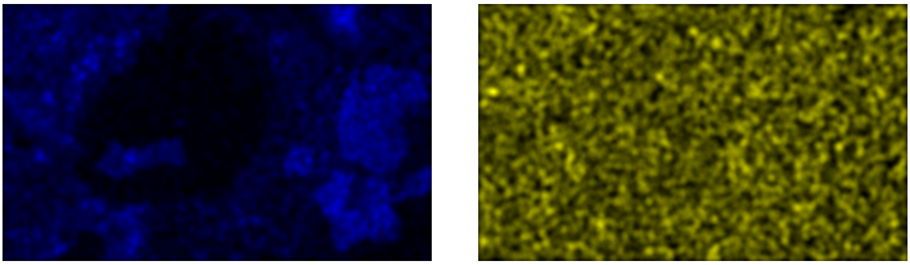

(e) Cl-map (K-line) (f) Pb-map ($M\alpha$-line)

Figure B.5: EDS data from the AP65-electrode in the AP65$_{0.8}$-cell.

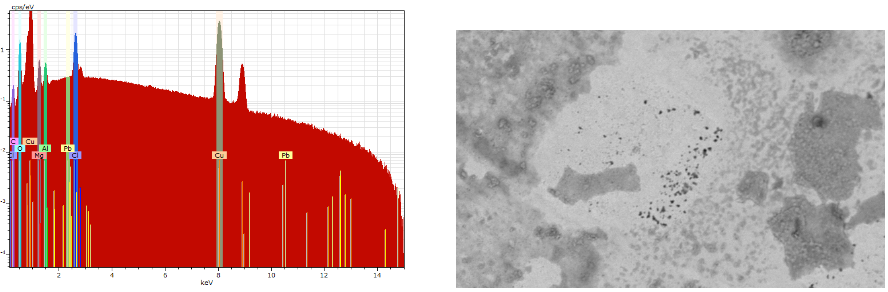

(a) EDS-spectra

(b) BSE-image

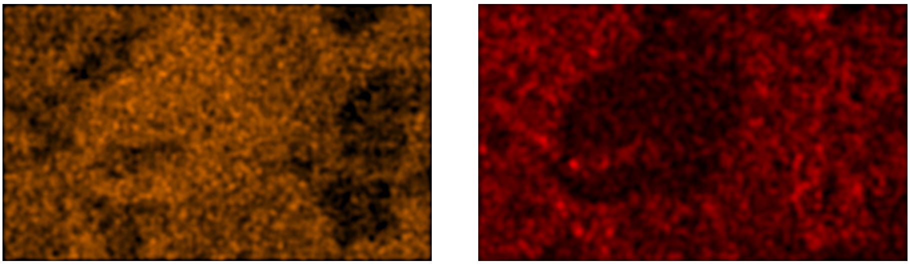

(c) Cu-map ($K\alpha$-line)

(d) Mg-map (K-line)

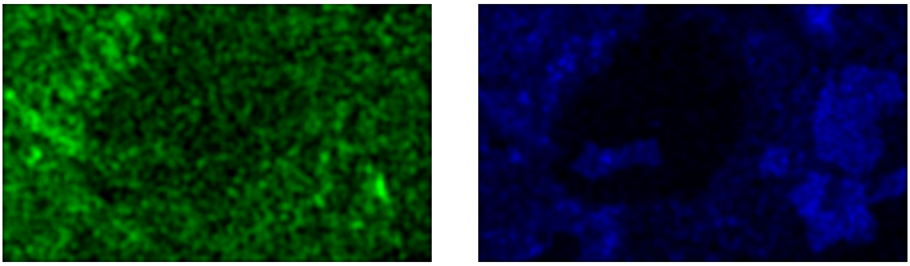

(e) Al-map (K-line)

(f) Cl-map ($K\alpha$-line)

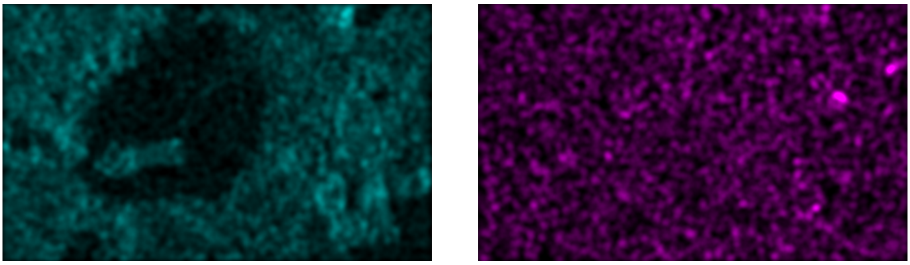

(g) O-map (K-line)

(h) C-map ($K\alpha$-line)

Figure B.6: EDS data from the Cu-electrode in the AP65$_{0.8}$-cell. Pb-lines are marked in the spectra, to shown that no signal from Pb is observed.